國立交通大學

電信工程研究所

碩 士 論 文

正交頻率多工訊號之低複雜度峰均值降低方法

Low-Complexity PAPR Reduction Schemes for OFDM Systems

研 究 生：陳至寧

指導教授：蘇育德　教授

中 華 民 國 一 百 年 八 月

正交頻率多工訊號之低複雜度峰均值降低方法

Low-Complexity PAPR Reduction Schemes for OFDM Systems

研 究 生：陳至寧　　Student：Chih-Ning Chen

指導教授：蘇育德　　Advisor：Dr. Tu T. Su

國 立 交 通 大 學

電信工程研究所

碩 士 論 文

A Thesis

Submitted to Institute of Communication Engineering

College of Electrical and Computer Engineering

National Chiao Tung University

in partial Fulfillment of the Requirements

for the Degree of

Master

in

Communication Engineering

August 2011

Hsinchu, Taiwan, Republic of China

中華民國一百年八月

正交頻率多工訊號之低複雜度峰均值降低之方法

學生:陳至寧　　指導教授:蘇育德　博士

國立交通大學電信工程研究所碩士班

摘　　要

由於正交頻率多工 (OFDM)信號會使傳送時間訊號產生高峰均值(PAPR)，讓系統的傳輸功率效能打了不少折扣。在許多種解決方案中，選擇性映射 (Selective Mapping) 及部分傳輸序列 (Partial Transmit Sequences)算是比較簡易可行的。然而，此兩種方法需要作多次的 IDFT，其運算複雜度仍高，為提升其可行性，簡化運算複雜度是必要的。現有大多數的簡化複雜度的方法似乎都沒有考慮到快速傅立葉轉換 (FFT)或反轉換（IFFT）的代數與硬體結構性質。我們認為上述兩種降低峰均值方法若能一併考慮快速傅立葉轉換的結構將有助於簡化其實現複雜度，提高其實用性。

在這篇論文中，我們依前述理念，提出新型的架構概念可以達到上述的目的。目前現有的選擇性映射及部分傳輸序列均可藉由我們提出的兩種方法，達到降低複雜度的目的。我們提的方法，除可降低運算複雜度之外，也能在相同複雜度的前提之下，降低更多的峰均值。此外，我們又提出了一個可以提早結束計算的機制，根據這個機制，可以節省更多的運算量。

Low-Complexity PAPR Reduction Schemes for OFDM Systems

Student : Chih-Ning Chen Advisor : Yu T. Su

Department of Communications Engineering

National Chiao Tung University

Abstract

One major problem with an orthogonal frequency division multiplexing (OFDM) system is high peak-to-average power ratio (PAPR) of the transmitter's output signals. To deal with it, several reduction scheme have been proposed and selective mapping (SLM) and partial transmit sequence (PTS) are two of them. Nevertheless, both two schemes incur high computational complexity and simplification is required. Although there are several works are devoted to the simplification, we find that most of them are designed without considering the structure of fast Fourier transform (FFT). It motives us to jointly design the PAPR reduction scheme and FFT.

In this thesis, we propose a concept to achieve this goal and several existed PAPR reduction schemes can be simplified with this concept. Here, two variant PAPR reduction schemes are considered and we will show that either the computational complexity can be reduced or we can get lower PAPR compared to the conventional schemes. In addition, a early stopping criterion is proposed to further reduce the computational complexity.

誌　　謝

對於論文得以順利完成，首先感謝我的指導教授 蘇育德博士。老師的諄諄教誨不只使我於通訊領域上有更深入的了解，生活上的指導也令我受益匪淺。感謝口試委員趙啟超教授、蘇賜麟教授、楊谷章教授以及李志鵬教授給予的寶貴意見，以補足這分論文的缺失與不足之處。

我還要感謝實驗室的劉人仰學長，在研究方面指導我，給予我很多很好的建議、觀念和經驗分享，幫助我的論文完成。另外，由衷感謝實驗室學長姐、同學及學弟妹在這兩年內的幫忙與鼓勵。

感謝一直在背後默默支持我的家人，他們的關心與鼓勵是我帶給了我無形的動力，僅獻上此論文，以代表我最深的敬意。

最後，感謝每一個幫助過我的人、一起歡笑奮鬥努力的朋友，感謝你們！

陳至寧謹致 于新竹國立交通大學

Contents

Chinese Abstract ii

English Abstract ii

Acknowledgements iv

Contents iv

List of Figures vi

List of Tables ix

1 Introduction 1

2 System Model and DFT/IDFT Architectures 4

2.1 Orthogonal Frequency Division Multiplexing 4

2.2 Peak-to-Average Power Ratio 6

2.3 Conventional Schemes for PAPR Reduction 8

2.3.1 Selective Mapping 8

2.3.2 Partial Transmit Sequence 10

2.4 Radix-r Algorithm 11

2.4.1 Decimation-in-Frequency Algorithm 12

2.4.2 Decimation-in-Time Algorithm 16

3 IDFT architecture aware PAPR reduction schemes I **21**

3.1 Proposed Algorithm 21

3.1.1 Corresponding SLM Scheme 22

3.1.2 Corresponding PTS Scheme 26

3.1.3 Proposed Stop Criterion 30

3.2 Performance Analysis and Comparison 35

3.2.1 Analysis of Computational Complexity 35

3.2.2 Simulation Results 35

3.3 Proposed Algorithm with Conversion Vectors 37

3.3.1 Brief introduction for LWW Scheme 37

3.3.2 Modified LWW Scheme with Proposed Stop Criterion 39

3.3.3 Analysis of Computational Complexity 40

3.3.4 Simulation Results 43

3.4 Transform Decomposition 45

4 IDFT architecture aware PAPR reduction schemes II **50**

4.1 Related work 50

4.2 Proposed New SLM and PTS Schemes 51

4.2.1 Scheme Description 51

4.2.2 Phase sequences of new SLM and PTS Schemes 55

4.3 Performance Analysis and Comparison 55

4.3.1 Computational Complexity Analysis 55

4.3.2 Simulation Results 57

5 Conclusion **63**

Bibliography **65**

List of Figures

2.1 Block diagram of an OFDM system. 5

2.2 Theoretical and simulated CCDF curves of the PAPR with $N = 16$ and $N = 1024$. 9

2.3 Block diagram of the SLM scheme. 10

2.4 Block diagram of the PTS scheme. 11

2.5 Flow graph of the DIF decomposition of an 8-point IDFT computation into two 4-point IDFTs together with the proper linear combination. . . 13

2.6 Flow graph of the complete DIF decomposition of an 8-point IDFT computation. 14

2.7 Flow graph of the basic butterfly computation for Fig. 2.6. 14

2.8 Flow graph of the simplified butterfly computation for Fig. 2.7. 15

2.9 Flow graph of the 8-point IDFT using the butterfly computation of Fig. 2.8. 15

2.10 Flow graph of the DIF decomposition of an N-point IDFT computation into $r \times (N/r)$-point IDFTs. 16

2.11 Flow graph of the DIT decomposition of an 8-point IDFT computation into two 4-point IDFTs. 18

2.12 Flow graph of the complete DIT decomposition of an 8-point IDFT computation. 19

2.13 Flow graph of the DIT of an N-point IDFT computation into r (N/r)-point IDFT computations. 20

3.1 Flow graph of radix-4 DIT decomposition of an NL-point IDFT computation into four $(NL/4)$-point IDFTs. 24
3.2 Flow graph of the radix-8 DIT of an NL-point IDFT computation into eight $(NL/8)$-point IDFTs. 28
3.3 Flow graph of the radix-r DIT decomposition of an NL-point IDFT computation into $r \times (NL/r)$-point IDFT computations. 31
3.4 Illustration of the proposed stop criterion (I). 32
3.5 Illustration of the proposed stop criterion (II). 33
3.6 Comparison of PAPR performance of Proposed SLM Scheme and conventional SLM Scheme. 38
3.7 Comparison of PAPR performance of Proposed PTS Scheme and conventional PTS Scheme. 39
3.8 Architecture of L&W Scheme I. 40
3.9 Architecture of modified convolution structure for generating candidate sequences. 41
3.10 Architecture of our proposed scheme with conversion vectors. 42
3.11 Comparison of PAPR reduction performance of the proposed modified schemes I and II, LWW schemes I and II, and conventional SLM schemes. 46
3.12 Comparison of PAPR reduction performance of the proposed modified scheme III, LWW scheme III, and conventional SLM scheme. 47
3.13 Comparison of PAPR reduction performance of the proposed modified schemes I and II, and the conventional PTS scheme. 48
3.14 Comparison of PAPR reduction performance of the proposed modified scheme III and the conventional PTS scheme. 49

4.1 Architecture of the proposed scheme. 52
4.2 Detailed architecture of the proposed scheme. 53

4.3 Block diagram of the proposed new SLM scheme with $v_D = [1, 4]$ and $P_D = [2, 8]$. 54
4.4 Comparison of the PAPR reduction performance of the proposed SLM Scheme, G&G SLM scheme and conventional SLM scheme. 59
4.5 Magnitude of an equivalent phase sequence of our scheme. 60
4.6 Magnitude of an equivalent phase sequence of the G&G SLM scheme. . . 61
4.7 Comparison of the BER performance of the proposed SLM Scheme and the G&G SLM scheme. 62

List of Tables

3.1 The Proposed Algorithm 34

3.2 Computational Complexity of Various Schemes (I) 36

3.3 Computational Complexity of Various Schemes (II) 36

3.4 Computational Complexity Ratio of the Proposed SLM Scheme with $N = 256$ 36

3.5 Computational Complexity Ratio of the Proposed PTS Schemes with $N = 256$ and $U = 8$. 37

3.6 Computational complexity of various SLM schemes (I) 43

3.7 Computational complexity of various SLM schemes (II) 43

3.8 Computational complexity of various PTS schemes (I) 43

3.9 Computational complexity of various PTS schemes (II) 44

3.10 Computational complexity ratio for Proposed SLM Schemes over the conventional SLM scheme with $N = 256$. 44

3.11 Computational complexity ratio for Proposed PTS Schemes over the conventional PTS scheme with $N = 256$ and $U = 8$. 45

4.1 Computational complexity of various SLM schemes (I) 57

4.2 Computational complexity of various SLM schemes (II) 57

4.3 Computational complexity ratio of the proposed SLM schemes with $N = 256$. 58

Chapter 1

Introduction

Orthogonal frequency division multiplexing (OFDM) has become a very popular transmission scheme for wideband communication systems due to its many desired properties. For instance, it has high spectral/power efficiencies, admits simple channel estimation and equalization, is compatible with other anti-fading methods and allows flexible resource allocation. With all these advantages, it suffers from one major drawback: high peak-to-average power ratio (PAPR) of the resulting time-domain waveforms. The high PAPR effect often forces the transmit power amplifier backoff to avoid significant nonlinear signal distortion.

Various techniques have been proposed to deal with this issue [1]. These methods can be classified into three categories. The first category can be referred to as the block coding scheme [2]. A subset of legitimate signals with lower PAPR is transmitted instead of using the whole signal space, and a pre-defined mapping rule between information bit stream and signal subset has to be set up.

The second category includes several signal distortion schemes. Among them, clipping [3] is the simplest–it basically clips those parts of the signal whose magnitude exceed the predetermined threshold. Nevertheless, as clipping suffers from in-band distortion and out-band radiation, it results in spectral efficiency reduction and error rate performance degradation. Active constellation extension (ACE) [4] clips signal in time-domain and forces frequency-domain components to stay within an extended region so that no

BER degradation will occur. For tone reservation (TR) [5], the transmitter does not send data on s small subset of subcarriers, and find the specific time-domain signal to be added to the original time-domain signal to lower the value of PAPR. Tone injection (TI) [5] adjusts frequency-domain signal by choosing transmitted signal from alternative signal points to reduce peaks in time-domain.

The last category involves different signal scrambling schemes. In selective mapping (SLM) [6], an input frequency domain data block is multiplied by several predetermined sequences to generate the alternative sequences, and the one with the lowest time domain PAPR is selected for transmission. In partial transmit sequences (PTS) [7], the input data block is partitioned into a number of disjoint subblocks, which are phase rotated by a set of phasors to produce a set of candidate sequences. The one with the lowest PAPR is chosen for transmission. Obviously, both SLM and PTS schemes need to perform multiple inverse fast Fourier transforms (IFFTs) and the associated computational complexity is often the main design concern that prevents their usages in a practical system.

In this thesis, we propose two new PAPR reduction approaches based on SLM and PTS schemes. In the first scheme, decimation-in-time radix-r IFFT algorithm is exploited to transform an NL-point IDFT into two consecutive $r \times (NL/r)$-point IDFT stages, with r being a adjusting parameter to produce different SLM and PTS alternatives. Unlike the conventional SLM and PTS schemes, phase sequences are applied to time-domain sequences and frequency-domain sequences respectively, phase sequences are multiplied to intermediate sequences between stage one and stage two. As a result, the calculation results of stage one are the same for all candidate sequences and just have to be calculated once for a given OFDM symbol. In addition, a stop criterion is also proposed to drop unnecessary calculations so that lower computational complexity is achieved and the same PAPR reduction performance as the conventional SLM or PTS schemes is provided.

It has been introduced in [12], the operations of IDFT can be replaced by conversion vectors. By performing circular convolution of IDFT of input data block and conversion vector with different number of right cyclic shift, a number of candidate sequences are generated. These conversion vectors are modified into our proposed scheme so that only $r \times (NL/r)$-point IDFTs are needed, and certain computational complexity is relieved due to the reason mentioned in preceding paragraph.

The second proposed scheme generalizes the two-stage decomposition to a multiple-stage DIT radix-r IFFT implementation in which the values of r of stage one and the remaining stages can be different. For this multiple-stage SLM or PTS approach, phase sequences are multiplied to intermediate sequences within IFFT operations at more than one stage. Since the phase sequence generations are different from that of [16, 17], better PAPR reduction performance is achieved with the same computational complexity. Compares with the conventional SLM and PTS schemes, it achieves a lower computational complexity at the cost of slightly PAPR performance degradation. In other words, with the same complexity, our scheme provides better PAPR reduction performance than that of conventional schemes.

The rest of the thesis is organized as follow. The ensuing chapter provides a general description of OFDM systems and the associated PAPR problem. Detail description of the conventional SLM and PTS schemes is given in Chapter 2. In Chapter 3 we present our first DIT radix-r IFFT based scheme and a stop criterion for early termination. We also present schemes that combine our algorithm and the conversion vector approach of [12] in this chapter. In Chapter 4, we introduce a scheme which utilizes multiple-stage DIT radix-r IFFT to further lower the computational complexity. Analysis of computational complexity and simulated PAPR curves of various approaches are provided in the related chapters. Finally, concluding remarks and suggestions for future studies are provided in Chapter 5.

Chapter 2

System Model and DFT/IDFT Architectures

2.1 Orthogonal Frequency Division Multiplexing

Nowadays high data rate is desired in many applications. However, as the symbol duration decreases with increasing data rate, single carrier systems suffer from severer intersymbol interference (ISI) caused by the dispersive fading of wireless channels or equivalently, frequency selective fading channels. Therefore, a technique called orthogonal frequency division multiplexing (OFDM) is introduced to cope with this problem.

The basic idea of OFDM is to divide the entire frequency selective fading channel into many narrowband flat fading subchannels. In other words, a high-rate data stream is split into several lower rate streams that are transmitted simultaneously over a number of subchannels, which can also be called subcarriers. Due to the increase of symbol duration for the lower rate streams, the relative amount of dispersion caused by the multi-path nature decreases. Furthermore, ISI can almost be completely eliminated with the aid of the cyclic prefix (CP) in which the OFDM symbol is cyclically extended to avoid intercarrier interference (ICI). The function of a CP is detailed later.

The block diagram of an OFDM system is provided in Fig. 2.1. The information bit stream is first encoded by a channel coding scheme (e.g. BCH code, convolutional code)

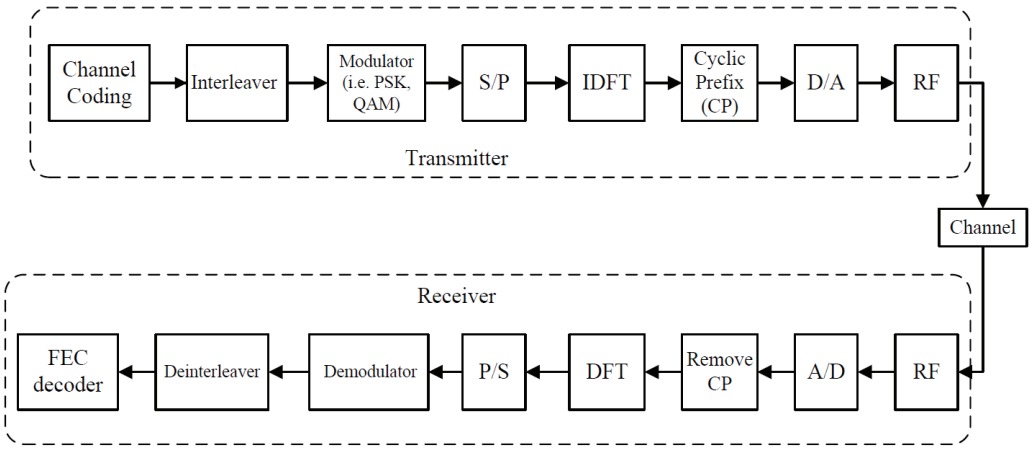

Figure 2.1: Block diagram of an OFDM system.

and then passed through an interleaver to increase the resistance to inferior frequency-selective channel conditions such as a deep fade. Serial-to-parallel (S/P) is used to generate the inputs of inverse discrete Fourier transform (IDFT) from the outputs of the modulator.

An OFDM symbol can be expressed as the sum of many independent signals modulated onto subcarriers. Let $\{X_k | k = 0, 1, \cdots, N-1\}$ denote a block of N complex data symbols modulated by phase shift keying (PSK) or quadrature amplitude modulation (QAM). The complex baseband representation of an OFDM symbol is given as

$$x(t) = \frac{1}{N} \sum_{k=0}^{N-1} X_k \exp\left(j2\pi k \Delta f t\right), \quad 0 \le t \le T, \tag{2.1}$$

where T is the OFDM symbol duration and $\Delta f = 1/T$ is the adjacent subcarrier separation. The discrete-time equivalent is the IDFT of $\{X_k\}$ given by the following, with time index t being replaced by sample number n,

$$x_n = \frac{1}{N} \sum_{k=0}^{N-1} X_k \exp\left(\frac{j2\pi nk}{N}\right), \quad n = 0, 1, \cdots, N-1, \tag{2.2}$$

where $\{x_n | n = 0, 1, \cdots, N-1\}$ is the time-domain sequence. In practice, the IDFT can be implemented efficiently by the inverse fast Fourier transform (IFFT) whose complexity can be reduced to $O(N \log_2(N))$ with the radix-2 algorithm.

In multipath channel, delayed replicas of the previous OFDM symbol lead to ISI between successive OFDM symbols. To eliminate the effects of ISI caused by the channel delay spread, a CP or guard interval is inserted between blocks of N IFFT coefficients, where the length of the CP is at least equal to that of the delay spread, such that multipath components from one symbol cannot interfere with the next symbol. The CP is simply a copy of the tail part of an OFDM symbol and can be attached to the front of the OFDM symbol. In this way, delayed replicas of the OFDM symbol always have an integer number of cycles within the FFT interval, as long as the delay spread is smaller than the length of CP or guard time. After appending the CP, the digital-to-analog converter (D/A) is involved to transform a discrete-time signal to an analog signal that passes to the radio frequency (RF) block. The RF block consists of up-converter, high power amplifier, and antenna. While the above-mentioned is the structure of an OFDM transmitter, the receiver is in a reverse operation with blocks having the inverse functions of those of the transmitter in the reverse order as depicted in Fig. 2.1.

2.2 Peak-to-Average Power Ratio

Since an OFDM symbol comprises a sum of modulated subcarriers, it is likely N sinusoids are added up coherently such that a large peak-to-average power ratio (PAPR) exists. When N signals are added with the same phase, N times peak power compare to average power is produced.

A large peak-to-average power ratio results in some disadvantages such as a reduced power efficiency of the power amplifier (PA). A large peak forces signal fall into the saturation region of the PA and causes nonlinear distortion. In such case, back-off is necessary for the power amplifier and its operating point is moved toward the origin to avoid signal from clipping. Hence, its power efficiency decreases proportionally with the back-off range. Even worse, nonlinear distortion may cause the degradation of bit-error rate (BER) performance. Therefore, a number of PAPR reduction schemes are proposed

to solve these problems.

While the discrete time PAPR of the transmit signal is defined as

$$PAPR = \frac{\max\limits_{0 \le n < N-1} |x_n|^2}{E\left[|x_n|^2\right]}, \tag{2.3}$$

an L-oversampling is needed to ensure a negligible approximation error if the discrete PAPR analysis is to be used to approximate analog waveforms. The L-oversampling can be implemented by taking an NL-point IFFT on data block $\mathbf{X}$ concatenated with $(L-1)N$ zeros, that is, $\mathbf{X} = [X_0, X_1, \cdots, X_{N-1}, 0, \cdots, 0]^T$. Therefore, the PAPR of the transmit signal can be rewritten as

$$PAPR = \frac{\max\limits_{0 \le n < NL-1} |x_n|^2}{E\left[|x_n|^2\right]}. \tag{2.4}$$

It is shown in [8, 9] that $L = 4$ can provide sufficiently accurate PAPR result. After knowing the drawbacks and the definition of PAPR, the measurement of it shall be introduced.

The complementary cumulative distribution function (CCDF) of the PAPR denotes the probability that the PAPR of a data block exceeds a given value is commonly used to measure the performance of PAPR reduction techniques. In [10], an approximate expression is derived for the CCDF of the PAPR for an OFDM symbol. From the central limit theorem we know that for a large value of N, the number of subcarriers for the OFDM system, each time-domain signal sample x_n is a circularly symmetric complex Gaussian random variable with a mean of zero and a variance of 1. As a result, the amplitude of an OFDM symbol is Rayleigh distributed while the power distribution becomes a central chi-square distribution of two degrees of freedom with a cumulative distribution function (CDF) given by

$$F(z) = 1 - \exp(-z). \tag{2.5}$$

CCDF of the PAPR per OFDM symbol, and this expression is given by

$$\begin{aligned} P(PAPR > z) &= 1 - P(PAPR \leq z) \\ &= 1 - F(z)^N \\ &= 1 - (1 - \exp(-z))^N \end{aligned} \tag{2.6}$$

Equation shown above is obtained by assuming time-domain samples, x_n, are mutually independent. Theoretical curves and simulated curves are plotted in Fig. 2.2. We can notice that for the case of small N, (2.6) cannot approximate the true behavior well since the Gaussian assumption does not hold. Besides, this expression is not accurate anymore when oversampling is applied. Hence, in the following chapters, simulated curves are used to compare the performance of various PAPR reduction techniques, where the closer the CCDF curve is to the vertical axis, the better its PAPR characteristic.

2.3 Conventional Schemes for PAPR Reduction

To reduce PAPR of OFDM systems, it is possible to eliminate high peak values due to the constructive interference of time-domain signals with an identical phase by phase rotation. There are two methods, based on the rotation of phases of the subcarriers of a given OFDM symbol, that are commonly used; specifically , the selective mapping (SLM) and partial transmit sequences (PTS) schemes.

2.3.1 Selective Mapping

In the SLM technique, the input data block $\mathbf{X} = [X_0, X_1, \cdots, X_{N-1}]^T$ is multiplied element-wise by U phase sequences $\mathbf{B}^{(u)} = [b_0^{(u)}, b_1^{(u)}, \cdots, b_{N-1}^{(u)}]^T, u = 1, 2, \cdots, U$, to generate a set of alternative sequences which contain the same information as the original input data block where the first phase sequence $\mathbf{B}^{(1)}$ is usually set to be an all-one sequence. Thus, the uth alternative sequence is $\mathbf{X}^{(u)} = [X_0 b_0^{(u)}, X_1 b_1^{(u)}, \cdots, X_{N-1} b_{N-1}^{(u)}]^T$. Each of these alternative sequences is operated by IDFT operation and becomes one of

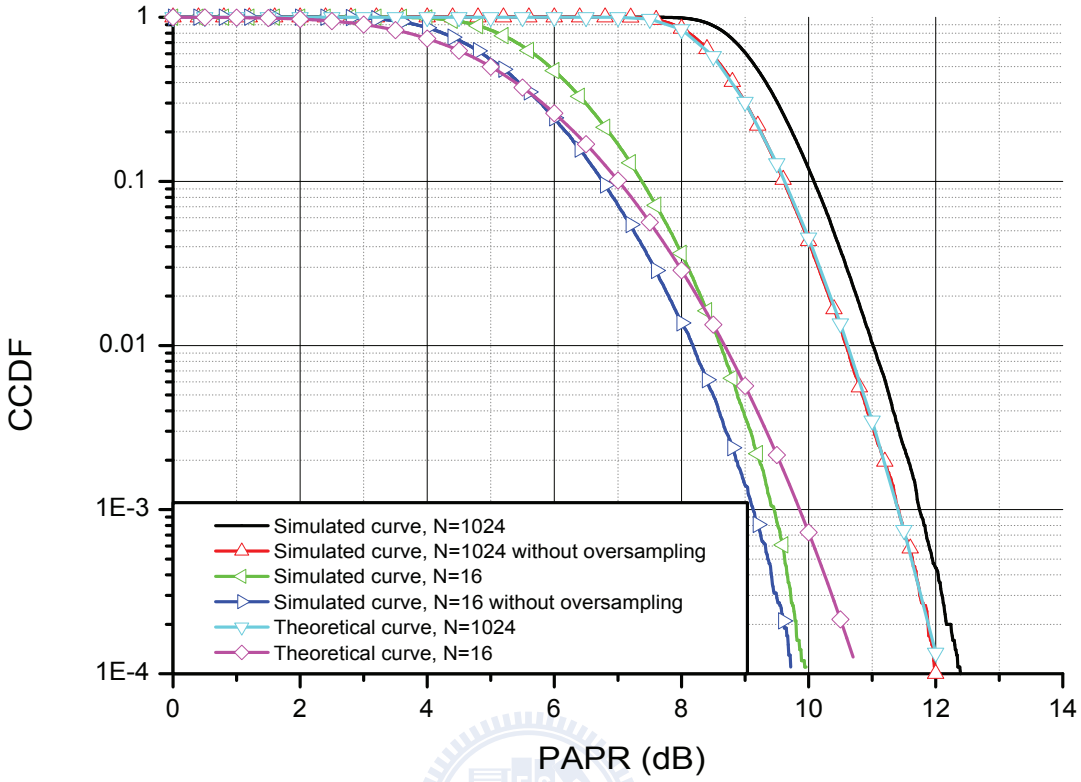

Figure 2.2: Theoretical and simulated CCDF curves of the PAPR with $N = 16$ and $N = 1024$.

the candidates

$$x_n^{(u)} = \frac{1}{N} \sum_{k=0}^{N-1} X_k b_k^{(k)} \mathrm{W}_N^{-kn}, \tag{2.7}$$

where $n = 0, 1, \ldots, N-1$ and $u = 1, 2, \ldots, U$, to choose from.

Among all the candidate sequences $\mathbf{X}^{(u)}$, only the one with the lowest PAPR is selected for transmission while the index u corresponding selected phase factor $\mathbf{B}^{(u)}$ also should be transmitted to the receiver as side information. For the implementation, the conventional SLM scheme needs U IDFT operations, and the number of required bits as side information is $\lceil \log_2 U \rceil$ for an input data block. This method is applicable to any type of modulation and any number of subcarriers. A block diagram of the SLM scheme is depicted in Fig. 2.3.

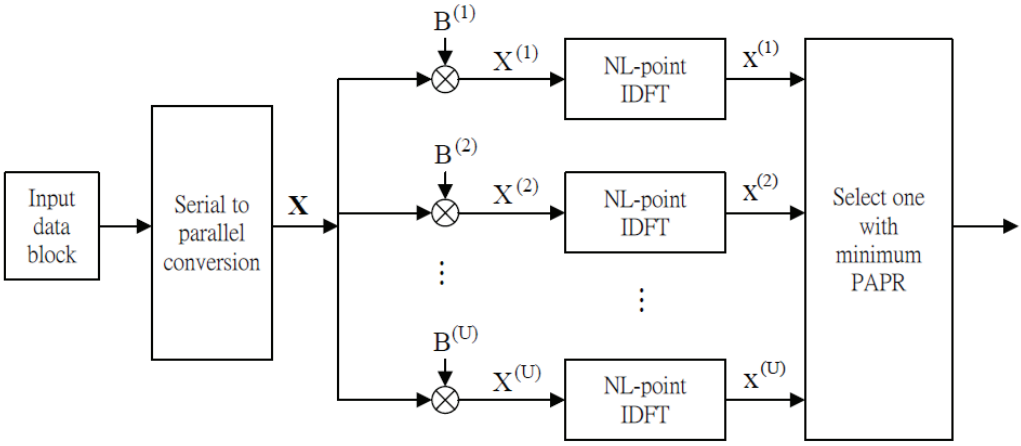

Figure 2.3: Block diagram of the SLM scheme.

2.3.2 Partial Transmit Sequence

In an OFDM system employing PTS technique to reduce PAPR, an input data block is partitioned into M disjoint subblocks $\mathbf{X}_m = [X_{m,0}, X_{m,1}, \ldots, X_{m,N-1}]^T$, $m = 1, 2, \cdots, M$, where only specific subcarriers in the mth subblock $\mathbf{X}_m$ are nonzero and the rest zero, i.e.,

$$\sum_{m=1}^{M} \mathbf{X}_m = \mathbf{X}. \tag{2.8}$$

Then, the subblocks $\mathbf{X}_m$ are trandformed into M time-domain partial transmit sequences, by NL-point IDFT operations, which are given as

$$\mathbf{x}_m = [x_{m,0}, x_{m,1}, \cdots, x_{m,NL-1}] = IDFT\{\mathbf{X}_m\}. \tag{2.9}$$

To reduce PAPR, these partial sequences are rotated by phase factors $\mathbf{b} = \{b_m = e^{j\theta_m} | m = 0, 1, \cdots, M-1\}$ independently. The PTS scheme is different from the SLM scheme in that phase factors are multiplied by the time-domain signal and it can be demonstrated by the linearity property of the IDFT operation:

$$\begin{aligned} \mathbf{x}'(\mathbf{b}) &= \sum_{m=1}^{M} b_m \cdot IDFT\{\mathbf{X}_m\} \\ &= \sum_{m=1}^{M} b_m \cdot \mathbf{x}_m. \end{aligned} \tag{2.10}$$

In order to determine the optimum phase vector $\mathbf{b}'$ which generates the candidate sequence with the lowest PAPR, the following is employed:

$$\mathbf{b}' = \arg\min_{\mathbf{b}} \left\{ \max_{0 \le n < NL-1} |x'_n| \right\}. \tag{2.11}$$

If W phase angles are allowed, e.g.,

$$\theta_m \in \left\{ \frac{2\pi i}{W} \mid i = 0, 1, \ldots, W-1 \right\}, \tag{2.12}$$

the number of all possible phase vectors is W^M. The block diagram of the PTS scheme is shown in Fig. 2.4. As we can see, in general, the conventional PTS scheme needs M IDFT operations for each input data block, and the number of required side information bits is $\lceil \log_2 W^M \rceil$.

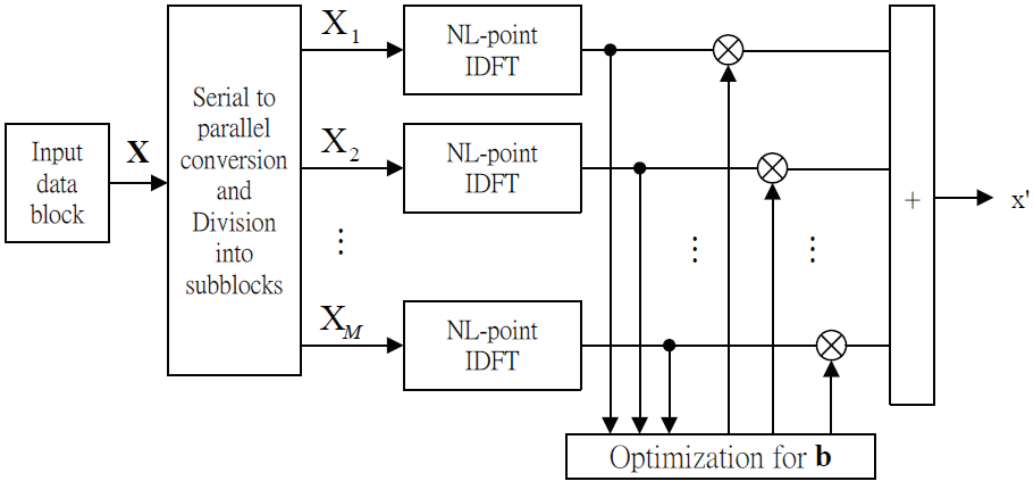

Figure 2.4: Block diagram of the PTS scheme.

Based on these two schemes, several new PAPR reduction schemes that are more efficient are proposed in the coming chapters.

2.4 Radix-r Algorithm

The IFFT algorithms are based on a divide-and-conquer approach which decomposes the computation of the IDFT of a N-length sequence into successively smaller IDFTs.

The fashion in which this principle is implemented results in a variety of different algorithms but all with comparable efficiency in computational speed. These algorithms are most efficient when the number of data points N is highly composite and can be written as $N = r_1 r_2 \cdots r_m$, where $r_1, \cdots, r_m$ are all integers. Specifically, when N equals to r^m, where r is called the radix of the IFFT algorithm, a regular structure can be seen in the IFFT algorithm.

The divide-and-conquer approach can be achieved by either decimation-in-time (DIT) or decimation-in-frequency (DIF). To illustrate these two concepts clearly, $N = 2^m$ (i.e. radix-2 algorithm)is considered in the following for the sake of simplicity.

2.4.1 Decimation-in-Frequency Algorithm

We first consider the DIF IFFT algorithm. It is mainly based on the decomposition of the computation into successively smaller IDFT operations and thus results in substantial efficiency boost. The decomposition is done by breaking sequence X_k down into successively smaller sequences. For $N = 2^m$, an even integer, we can compute x_n by dividing the sequence X_k into two $(N/2)$-point sequences where one consists of the even-numbered points and the odd-numbered points of X_k. With x_n given by

$$x_n = \frac{1}{N} \sum_{k=0}^{N-1} X_k \mathrm{W}_N^{-nk}, \quad n = 0, 1, \cdots, N-1, \tag{2.13}$$

where $\mathrm{W}_N = e^{-j2\pi/N}$ and dividing X_k into its even-numbered and odd-numbered halves, (2.13) becomes

$$\begin{aligned} x_n &= \frac{1}{N} \left(\sum_{k \text{ even}} X_k \mathrm{W}_N^{-nk} + \sum_{k \text{ odd}} X_k \mathrm{W}_N^{-nk} \right) \\ &= \frac{1}{N} \left(\sum_{s=0}^{(N/2)-1} X_{2s} \mathrm{W}_N^{-2sn} + \sum_{s=0}^{(N/2)-1} X_{2s+1} \mathrm{W}_N^{-(2s+1)n} \right) \\ &= \frac{1}{N} \left(\sum_{s=0}^{(N/2)-1} X_{2s} (\mathrm{W}_N^2)^{-sn} + \mathrm{W}_N^{-n} \sum_{s=0}^{(N/2)-1} X_{2s+1} (\mathrm{W}_N^2)^{-sn} \right) \end{aligned} \tag{2.14}$$

where the second equality is due to the substitution of variables $k = 2s$ for k even and $k = 2s + 1$ for k odd.

It can be noted that each of the sums in (2.14) denotes an $(N/2)$-point IDFT with the first being the IDFT of the even-numbered points and the second that of the odd-numbered points of the original input data sequence. After the two IDFTs are computed, they are combined linearly according to (2.14) to generate the N-point IDFT x_n. These procedures can be illustrated by Fig. 2.5, where $N = 8$ is taken as an example, and can be repeated recursively until reaching 2-point IDFTs. A 2-point IDFT consists only of additions and subtractions of two points. and requires $m = \log_2 N$ stages of computations. Figure 2.6 depicts the complete DIF decomposition of an 8-point IDFT computation with $m = 3$ stages. We note that each stage has N complex multiplica-

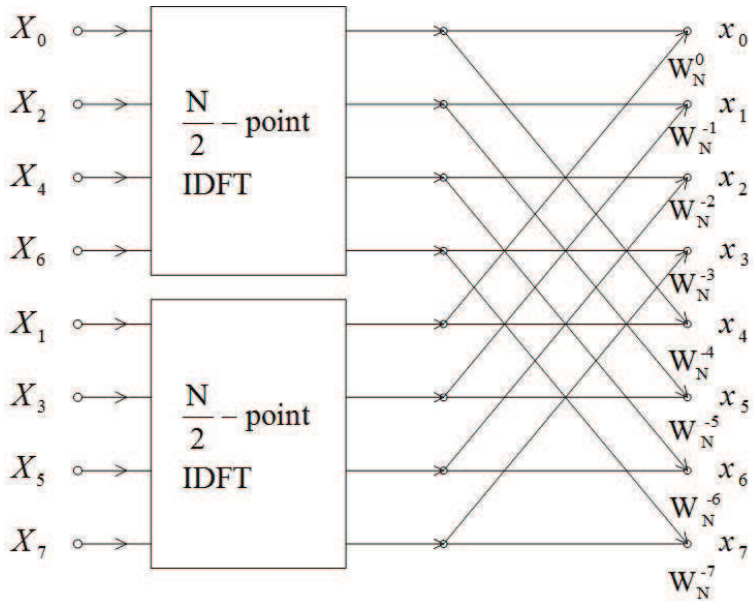

Figure 2.5: Flow graph of the DIF decomposition of an 8-point IDFT computation into two 4-point IDFTs together with the proper linear combination.

tions and N complex additions. Since there are $\log_2 N$ stages, we have in total $N \log_2 N$ complex multiplications and $N \log_2 N$ complex additions. Compared to the direct computation of IDFT (2.13), which requires N^2 complex multiplications and $N(N-1)$ complex additions, substantial calculations are saved.

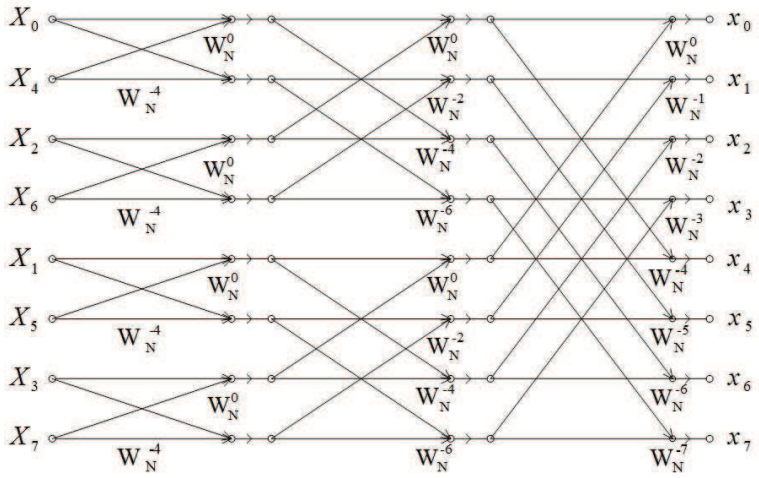

Figure 2.6: Flow graph of the complete DIF decomposition of an 8-point IDFT computation.

The amount of computation can be further reduced by exploiting the symmetry and periodicity of the complex coefficient W_N^{-n}. We note that the basic computation to obtain a pair of values in one stage from a pair of values in the preceding stage can be visualized by Fig. 2.7. From (2.14) and Fig. 2.6, it can be observed that the coefficients that linearly combine X_k's are always powers of W_N and exponents are separated by $N/2$. Due to the symmetry property of W_N, Fig. 2.7 can be transformed into Fig. 2.8.

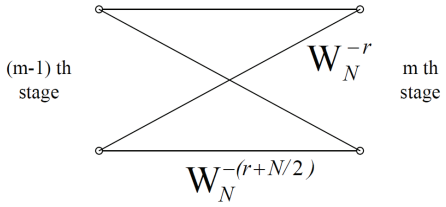

Figure 2.7: Flow graph of the basic butterfly computation for Fig. 2.6.

Accordingly, the computation of Fig. 2.7 can be simplified to Fig. 2.8, i.e. the required complex multiplication number is reduced from two to only one. Hence, by using the simplified form of the butterfly operation in Fig. 2.8, the total number of complex multiplications is $(N/2)\log_2 N$ and that of complex additions remains unchanged as $N\log_2 N$. The simlified version of Fig. 2.6 is given in Fig. 2.9.

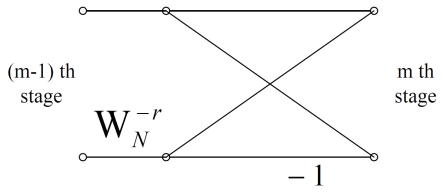

Figure 2.8: Flow graph of the simplified butterfly computation for Fig. 2.7.

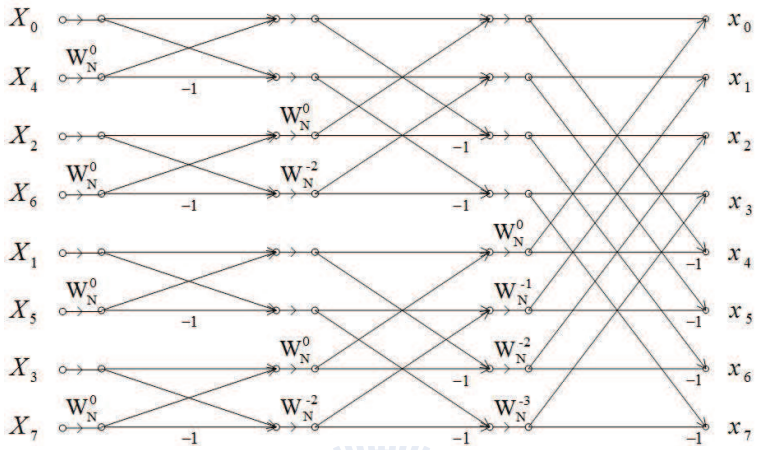

Figure 2.9: Flow graph of the 8-point IDFT using the butterfly computation of Fig. 2.8.

As for general cases other than $r = 2$, DIF IFFT can be implemented by dividing the frequency domain components into r subsets

$$\begin{aligned}
&\{X_{rs}\}_{s=0}^{NL/r-1};\\
&\{X_{rs+1}\}_{s=0}^{NL/r-1};\\
&\quad\vdots\\
&\{X_{rs+(r-1)}\}_{s=0}^{NL/r-1},
\end{aligned}$$

and (2.14) can be generalized to

$$\begin{aligned}
x_n \;=\; \frac{1}{N}\Bigg(&\sum_{s=0}^{(N/r)-1} X_{rs}(W_N^r)^{-sn} + W_N^{-n}\sum_{s=0}^{(N/r)-1} X_{rs+1}(W_N^r)^{-sn} + \cdots\\
&+W_N^{-(r-1)n}\sum_{s=0}^{(N/r)-1} X_{rs+(r-1)}(W_N^r)^{-sn}\Bigg). \qquad (2.15)
\end{aligned}$$

The flow graph of (2.15) is demonstrated in Fig. 2.10, and those $r \times (N/r)$-point IDFT can also be decomposed recursively in a similar manner as mentioned above into $\log_r N$ stages.

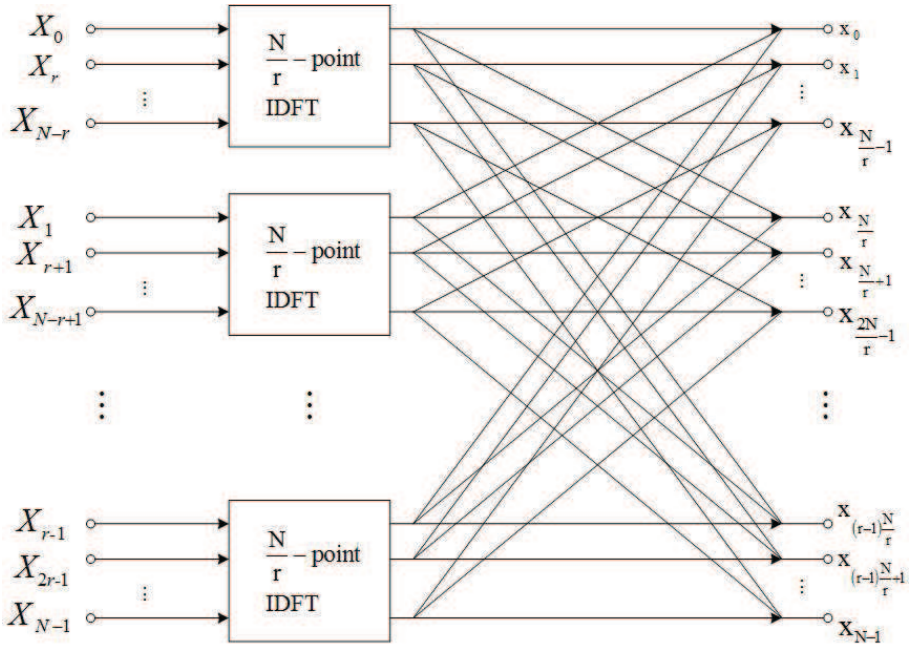

Figure 2.10: Flow graph of the DIF decomposition of an N-point IDFT computation into $r \times (N/r)$-point IDFTs.

2.4.2 Decimation-in-Time Algorithm

On the other hand, the DIT algorithm is organized in exactly the opposite manner of that of the DIF algorithm. In other words, while the latter computes IDFT by forming smaller subsequences of the input sequence X_k with some specific order, the IDFT computation based on DIT divides the output sequence x_n into successively smaller subsequences and is introduced subsequently.

Similarly, without loss of generality, we consider the case when $r = 2$ for the convenience of the explanation of the DIT algorithm. To construct DIT algorithms, let us consider computing separately the even-numbered *time-domain* samples and those odd-numbered. Again, starting form (2.13), we obtain the even-numbered time-domain

samples as

$$x_{2s} = \frac{1}{N}\sum_{k=0}^{N-1} X_k \mathrm{W}_N^{-k(2s)}, \quad s = 0, 1, \cdots, N/2-1, \tag{2.16}$$

which obviously can be expressed as

$$\begin{aligned} x_{2s} &= \frac{1}{N}\left(\sum_{k=0}^{(N/2)-1} X_k \mathrm{W}_N^{-k(2s)} + \sum_{k=N/2}^{N-1} X_k \mathrm{W}_N^{-k(2s)}\right). &(2.17)\\ &= \frac{1}{N}\left(\sum_{k=0}^{(N/2)-1} X_k \mathrm{W}_N^{-k(2s)} + \sum_{k=0}^{(N/2)-1} X_{k+N/2} \mathrm{W}_N^{-(k+N/2)2s}\right). &(2.18)\end{aligned}$$

Similarly, the odd-numbered time-domain samples are given by

$$x_{2s+1} = \frac{1}{N}\sum_{k=0}^{N-1} X_k \mathrm{W}_N^{-k(2s+1)}, \quad s = 0, 1, \cdots, N/2-1, \tag{2.19}$$

and can be rearrange to

$$\begin{aligned} x_{2s+1} &= \frac{1}{N}\left(\sum_{k=0}^{(N/2)-1} X_k \mathrm{W}_N^{-k(2s+1)} + \sum_{k=N/2}^{N-1} X_k \mathrm{W}_N^{-k(2s+1)}\right) \\ &= \frac{1}{N}\left(\sum_{k=0}^{(N/2)-1} X_k \mathrm{W}_N^{-k(2s+1)} + \sum_{k=0}^{(N/2)-1} X_{k+N/2} \mathrm{W}_N^{-(k+N/2)(2s+1)}\right). &(2.20)\end{aligned}$$

Because of the periodicity of W_N^{-2sk} and $\mathrm{W}_N^2 = \mathrm{W}_{N/2}$, $\mathrm{W}_N^{-(N/2)2s} = 1$, and $\mathrm{W}_N^{-N/2} = -1$,

$$\mathrm{W}_N^{-2s(k+N/2)} = \mathrm{W}_N^{-2sk}\mathrm{W}_N^{-sN} = \mathrm{W}_N^{-2sk}, \tag{2.21}$$

and (2.18) and (2.20) can be rewritten as

$$\begin{aligned} x_{2s} &= \frac{1}{N}\sum_{k=0}^{(N/2)-1} \left(X_k + X_{k+N/2}\right) \mathrm{W}_{N/2}^{-sk} &(2.22)\\ x_{2s+1} &= \frac{1}{N}\sum_{k=0}^{(N/2)-1} \left(X_k - X_{k+N/2}\right) \mathrm{W}_N^{-k}\mathrm{W}_{N/2}^{-ks}, &(2.23)\end{aligned}$$

where $s = 0, 1, \cdots, N/2-1$. It can be noticed that both (2.22) and (2.23) are the $(N/2)$-point IDFT of two $(N/2)$-length sequences, which are respectively obtained by adding the first and the last half of the input sequence element-by-element for the former and subtracting the last half from the first half followed by the multiplication of W_N^{-k}

for the latter. Thus, the IDFT can be computed by forming two sequences based on the brackets in the summations of (2.22) and (2.23), then computing the $(N/2)$-point IDFTs of these two sequences to obtain the even-numbered and the odd-numbered time-domain samples. The procedure discussed in above is illustrated in Fig. 2.11 for the case of an 8-point IDFT.

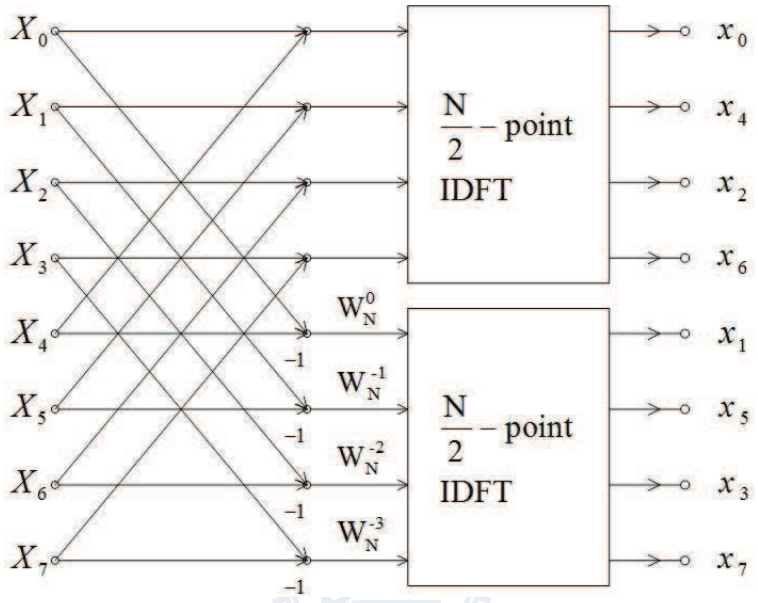

Figure 2.11: Flow graph of the DIT decomposition of an 8-point IDFT computation into two 4-point IDFTs.

Analogous to what have beeb seen in the DIF decomposition, the process of (2.22) and (2.23) can be done recursively for the smaller size of IDFTs (i.e. (N/2)-point IDFTs). This is realized by combining the first and the last half of the input points, which are of length $N/4$ for each $(N/2)$-point IDFTs led in (2.22) and (2.23) and then computing $(N/4)$-point IDFTs. This process can be done until reaching 2-point IDFT. The number of arithmetic operations involved $(N/2)\log_2 N$ complex multiplications and $N\log_2 N$ complex additions, thus making its computational complexity identical to that of the DIF one. For the 8-point example, the corresponding flow graph of the complete DIT decomposition is shown in Fig. 2.12.

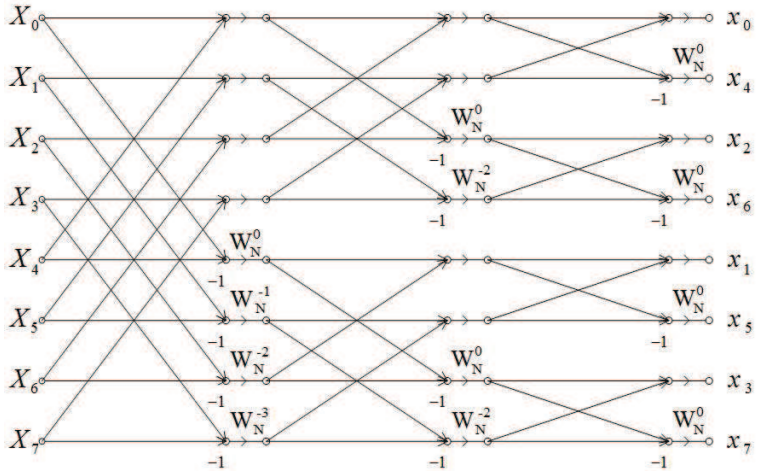

Figure 2.12: Flow graph of the complete DIT decomposition of an 8-point IDFT computation.

For general r's, we may consider the time-domain sequence x_n in r batches as

$$\begin{aligned} &\{x_{rn}\}_{n=0}^{N/r-1}; \\ &\{x_{rn+1}\}_{n=0}^{N/r-1}; \\ &\vdots \\ &\{x_{rn+(r-1)}\}_{n=0}^{N/r-1}, \end{aligned}$$

and the IDFT expression can be rewritten as

$$x_{rn+n_0} = \sum_{k=0}^{\frac{N}{r}-1} \left(\sum_{q=0}^{r-1} X_{k+\frac{qN}{r}} \mathrm{W}_N^{-\left(\frac{qN}{r}\right)n_0} \right) \mathrm{W}_N^{-k(rn+n_0)} \tag{2.24}$$

where $n = 0, 1, \ldots, N/r-1$ and $n_0 = 0, 1, \ldots, r-1$ is the index of the butterfly outputs. The flow graph is summarized in Fig. 2.13.

To conclude this section, we examine the tendency of the two decomposition methods as the computation moves from a former stage to a latter one. Specifically, the DIT IFFT algorithm successively decomposes larger IDFTs into smaller IDFTs while the DIF-based one performs the opposite, i.e., it combines smaller IDFTs into larger IDFTs. Therefore, the DIF IFFT algorithm needs to perform all the IDFTs in each stage before deriving a single time-domain sample whereas it is not the case for the DIT-based one. Only one

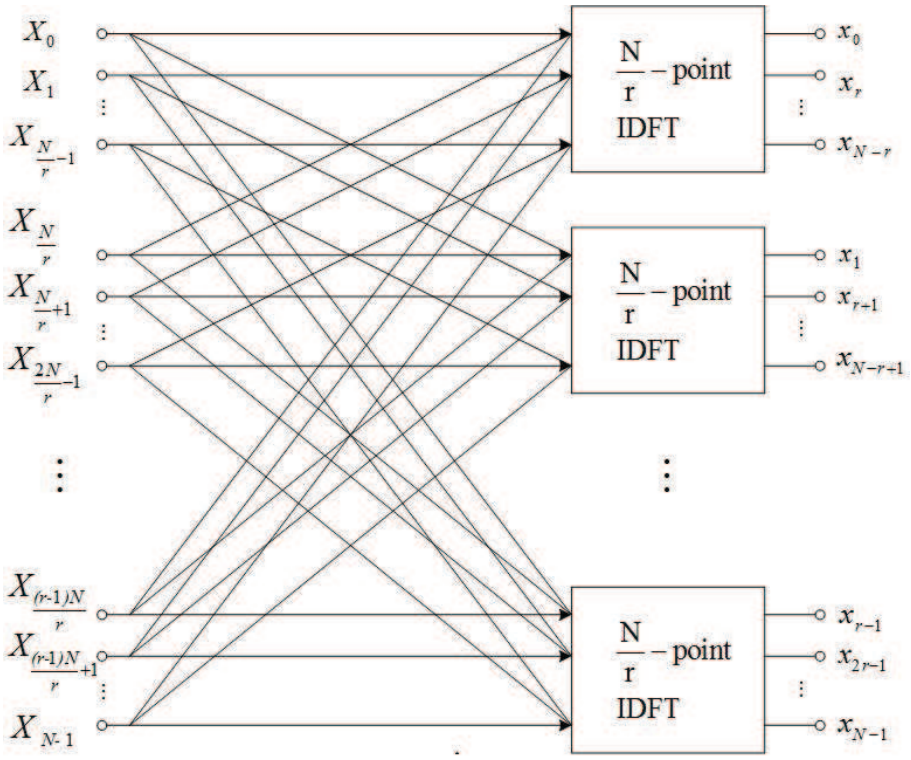

Figure 2.13: Flow graph of the DIT of an N-point IDFT computation into r (N/r)-point IDFT computations.

of the IDFTs in each stage is required to obtain a single output. This nice property of the DIT-based IFFT enables an early discard of unsuitable candidates before obtaining its whole output samples.

Chapter 3

IDFT architecture aware PAPR reduction schemes I

3.1 Proposed Algorithm

In the proposed algorithm, we take the radix-r DIT IFFT algorithm introduced in the previous subsection as the basic structure to develop a novel scheme that can reduce the computational complexity for PAPR reduction. Although N-point IDFT can be decomposed into $\log_2 N$ stages until reaching 2-point IDFT, here we exploit two stages only and visualize the structure in Fig. 2.13. The most important step of our construction is the selection of the value of r for radix-r at the first stage, because different such values of can result in different corresponding schemes for PAPR reduction such as the SLM and PTS methods. Hence, we will introduce two categories of values of r which respectively lead to the corresponding SLM and PTS schemes with L-oversampling employed. By taking some properties of the L-oversampling into account, we suggest some efficient algorithms. The way how our proposal reduces the complexity will also be mentioned in the subsequent discussions.

3.1.1 Corresponding SLM Scheme

In the rest of this thesis, the operation of L-oversampling interpreted as the IDFT of an data block $\mathbf{X}$ padded with $(L-1)N$ zeros, and the length of the IDFT input sequence becomes NL. Also note that as discussed previously, the oversampling of $L = 4$ folds is sufficient to provide accurate PAPR approximations in general and thus will be adopted throughout this work. Most importantly, efficient algorithms will be developed under this adoption.

As mentioned above, different values of r at the first stage result in distinct corresponding schemes for PAPR reduction. Specifically, if $r = L$ ($L = 4$) is chosen, the proposed algorithm can equivalently correspond to the SLM scheme, which rotates phases subcarrier-wise to lower the PAPR value of an input data block. As will be introduced later, when the radix-4 DIT-based IFFT is taken as the basic building block of our proposed algorithm, the corresponding SLM scheme can be obtained. Accordingly, an NL-point time-domain samples are partitioned into four subsets where each subset is the output samples of an $(NL/4)$-point IDFT. The mathematical expression of the output samples of the first $(NL/4)$-point IDFT is given as

$$x_{4s} = \frac{1}{NL} \sum_{k=0}^{NL-1} X_k \mathrm{W}_{NL}^{-(4s)k}, \quad s = 0, 1, \cdots, NL/4 - 1, \tag{3.1}$$

and can be expressed as

$$x_{4s} = \frac{1}{NL} \left(\sum_{k=0}^{\frac{NL}{4}-1} X_k \mathrm{W}_{NL}^{-k(4s)} + \sum_{k=\frac{NL}{4}}^{\frac{NL}{2}-1} X_k \mathrm{W}_{NL}^{-k(4s)} + \sum_{k=\frac{NL}{2}}^{\frac{3NL}{4}-1} X_k \mathrm{W}_{NL}^{-k(4s)} + \sum_{k=\frac{3NL}{4}}^{N-1} X_k \mathrm{W}_{NL}^{-k(4s)} \right) \tag{3.2}$$

With substitutions of variables in the last three summation in (3.2), we obtain

$$\begin{aligned} x_{4s} &= \frac{1}{NL}\left(\sum_{k=0}^{\frac{NL}{4}-1} X_k \mathrm{W}_{NL}^{-k(4s)} + \sum_{k=0}^{\frac{NL}{4}-1} X_{k+\frac{NL}{4}} \mathrm{W}_{NL}^{-(k+\frac{NL}{4})(4s)} \right. \\ &\quad \left. \sum_{k=0}^{\frac{NL}{4}-1} X_{k+\frac{NL}{2}} \mathrm{W}_{NL}^{-(k+\frac{NL}{2})(4s)} + \sum_{k=0}^{\frac{NL}{4}-1} X_{k+\frac{3NL}{4}} \mathrm{W}_{NL}^{-(k+\frac{3NL}{4})(4s)} \right) \\ &= \frac{1}{NL} \sum_{k=0}^{\frac{NL}{4}-1} \left(X_k + X_{k+\frac{NL}{4}} + X_{k+\frac{NL}{2}} + X_{k+\frac{3NL}{4}} \right) \mathrm{W}_{NL}^{-k(4s)}. \end{aligned} \tag{3.3}$$

From (3.3), it can be noticed that the input samples of $(NL/4)$-point IDFT is linear combination among four components of L-oversampled input data sequence and there is an interval of $NL/4$ between adjacent components. Similarly, output samples of the rest three $(NL/4)$-point IDFTs are given as

$$x_{4s+1} = \frac{1}{NL} \sum_{k=0}^{\frac{NL}{4}-1} \left(X_k + jX_{k+\frac{NL}{4}} - X_{k+\frac{NL}{2}} - jX_{k+\frac{3NL}{4}} \right) \mathrm{W}_{NL}^{-k} \mathrm{W}_{NL}^{-k(4s)}; \tag{3.4}$$

$$x_{4s+2} = \frac{1}{NL} \sum_{k=0}^{\frac{NL}{4}-1} \left(X_k - X_{k+\frac{NL}{4}} + X_{k+\frac{NL}{2}} - X_{k+\frac{3NL}{4}} \right) \mathrm{W}_{NL}^{-2k} \mathrm{W}_{NL}^{-k(4s)}; \tag{3.5}$$

$$x_{4s+3} = \frac{1}{NL} \sum_{k=0}^{\frac{NL}{4}-1} \left(X_k - jX_{k+\frac{NL}{4}} - X_{k+\frac{NL}{2}} + jX_{k+\frac{3NL}{4}} \right) \mathrm{W}_{NL}^{-3k} \mathrm{W}_{NL}^{-k(4s)} \tag{3.6}$$

where, similar to (3.3), each input samples of them can be obtained by a linear combination among four interleaved components of the length-NL zero-padded input data sequence. The flow graph of (3.3) – (3.6) are illustrated in Fig. 3.1. The different part of these four subsets is the weighting for each components in summations and for each $(NL/4)$-point IDFT, the weighting $\mathrm{W}_{NL}^{-kn_0}$ multiplied on the input sample is required, where $n_0 = 0, 1, 2, 3$ denotes the index of $(NL/4)$-point IDFT.

Due to the fact that $3N$ zeros are padded at the end of the original sequence to achieve 4-oversampling, only the first element (X_k) in the brackets of (3.3) – (3.6) is nonzero while the rest three elements ($X_{k+\frac{NL}{4}}, X_{k+\frac{NL}{2}}$, and $X_{k+\frac{3NL}{4}}$) zero. Hence, for these four $(NL/4)$-point IDFTs, the length-$\frac{NL}{4}$ input frequency-domain samples are the

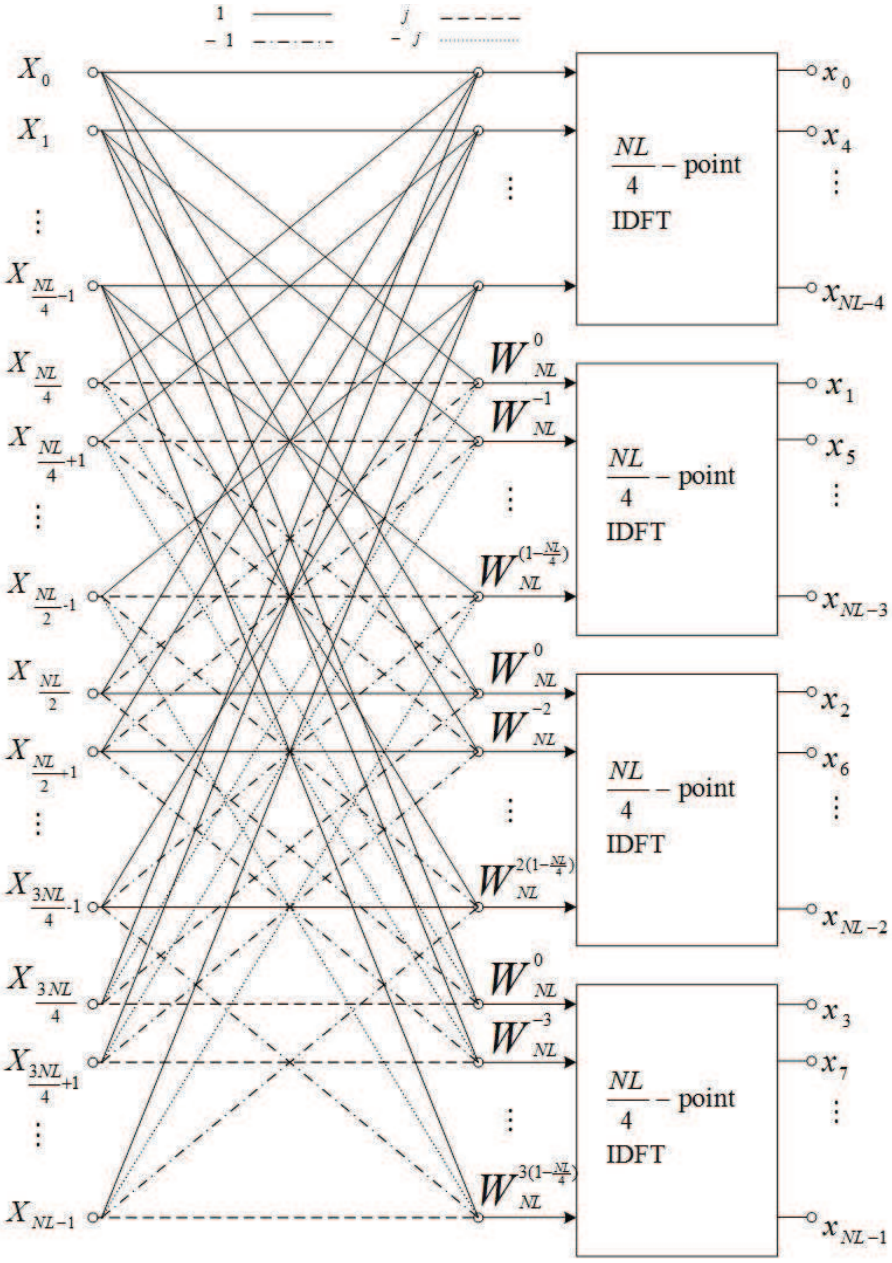

Figure 3.1: Flow graph of radix-4 DIT decomposition of an NL-point IDFT computation into four $(NL/4)$-point IDFTs.

same as the original input data block $\mathbf{X} = [X_0, X_1, \cdots, X_{N-1}]^T$ of length N when the weighting $\mathrm{W}_{NL}^{-kn_0}$ is not considered. After the process of four $(NL/4)$-point IDFTs, the length-NL time-domain samples can be obtained.

Now, the question is, how do we map this case in which radix-4 is considered at the first stage into the corresponding SLM scheme? The key is the position where the phase sequences are multiplied with the input data block $\mathbf{X}$. In the proposed algorithm, phase rotation occurs at the input sequences of the four $(NL/4)$-point IDFTs. In other words, phase sequences which generate candidate sequences are multiplied by the original input sequence of the four $(NL/4)$-point IDFTs (3.3) – (3.6) or, equivalently, multiplied with the data block $\mathbf{X}$ and then with different $\mathrm{W}_{NL}^{-kn_0}$ for different $(NL/4)$-point IDFTs. Therefore, the frequency-domain representation of the u-th candidate sequence can be expressed as

$$\mathbf{X}^{(u)} = \mathbf{X}\mathbf{B}^{(u)} \stackrel{def}{=} [X_0 b_0^{(u)}, X_1 b_1^{(u)}, \cdots, X_{N-1} b_{N-1}^{(u)}]^T \tag{3.7}$$

where $u = 1, 2, \cdots, U$, U is the number of phase sequences, and $\mathbf{B}^{(u)} = [b_0^{(u)}, b_1^{(u)}, \cdots, b_{N-1}^{(u)}]^T$ is the uth phase sequence. Additionally, there are different weightings $\mathrm{W}_{NL}^{-kn_0}, n_0 \in \{0, 1, 2, 3\}$ have to be multiplied prior or after $\mathbf{X}$ is multiplied by $\mathbf{B}^{(u)}$ for different $(NL/4)$-point IDFTs.

It can be noted from (3.7) that the subcarrier-wise multiplication of the phase factors and the input data block $\mathbf{X}$ makes our proposal identical to and be regarded as the conventional SLM scheme where $r = L$ $(L = 4)$. Furthermore, since phase sequences can be multiplied after the data $\mathbf{X}$ is scaled by weightings $\mathrm{W}_{NL}^{-kn_0}$, we are able to improve the conventional SLM scheme by the following: treating the calculation of the original inputs of the four $(NL/4)$-point IDFTs (3.3) – (3.6) as the first stage, and the multiplication of these input with $\mathbf{B}^{(u)}$ the second. The computation result at the first stage of a specific OFDM symbol can be calculated only *once* and stored and reused for U phase sequences at the second stage. Consequently, as opposed to the conventional SLM method, the proposed possesses lower computational complexity while preserves the same PAPR

reduction performance with the same number of subcarriers and phase sequences.

As a final remark, we should mention that as long as $NL/4$ equals to a power of some r', we can implement $(NL/4)$-point IDFTs efficiently by the radix-r' IFFT where $r' = 2$ is most commonly used and will be adopted in our simulations.

3.1.2 Corresponding PTS Scheme

In this subsection, we propose an algorithm that corresponds to a complexity-reduced PTS implementation. Similarly, the required operations to derive the L-oversampled IDFT of input data block $\mathbf{X}$ is performed here. Again, as mentioned, the oversampling of 4-fold (i.e. 4-oversampling) is sufficient to accurately approximate the PAPR value of the time-domain signal that carries data $\mathbf{X}$.

It has been mentioned in the beginning of this section that different values of r for radix-r at the first stage result in diverse corresponding schemes for PAPR reduction. In the following discussion, $r > L$ $(L = 4)$ is chosen to map this proposed algorithm to the corresponding PTS scheme, where r is a multiple of 4. For the conventional PTS scheme, the input data block is partitioned into M subblocks and phase rotation is operated block-wise, i.e., subcarriers belong to the same subblock are multiplied by the same phase factor to reduce the value of PAPR of the input data block $\mathbf{X}$.

We first claim that the radix-r DIT IFFT algorithm with $r > L$ and r being any multiple of 4 is the basic structure to correspond to a PTS scheme, without loss of generality, we may take $r = 8$ as an example to illustrate our proposal. According to the discussion in Section 2.4.2, NL-point time-domain samples are divided into eight subsets where each of them forms output samples of an $(NL/8)$-point IDFT. The mathematical expression of the radix-8 DIT IFFT algorithm is given by

$$x_{8s} = \frac{1}{NL} \sum_{k=0}^{NL-1} X_k \mathrm{W}_{NL}^{-k(8s)}, \quad s = 0, 1, \cdots, NL/8 - 1, \tag{3.8}$$

which is the expression of the first $(NL/8)$-point IDFT output and can be rewritten as

$$\begin{aligned} x_{8s} &= \frac{1}{NL}\sum_{k=0}^{\frac{NL}{8}-1}\Big(X_k \mathrm{W}_{NL}^{-k(8s)} + X_{k+\frac{NL}{8}}\mathrm{W}_{NL}^{-(k+\frac{NL}{8})(8s)} + X_{k+\frac{NL}{4}}\mathrm{W}_{NL}^{-(k+\frac{NL}{4})(8s)} + \\ &\quad X_{k+\frac{3NL}{8}}\mathrm{W}_{NL}^{-(k+\frac{3NL}{8})(8s)} + X_{k+\frac{NL}{2}}\mathrm{W}_{NL}^{-(k+\frac{NL}{2})(8s)} + X_{k+\frac{5NL}{8}}\mathrm{W}_{NL}^{-(k+\frac{5NL}{8})(8s)} + \\ &\quad X_{k+\frac{3NL}{4}}\mathrm{W}_{NL}^{-(k+\frac{3NL}{4})(8s)} + X_{k+\frac{7NL}{8}}\mathrm{W}_{NL}^{-(k+\frac{7NL}{8})(8s)}\Big) \\ &= \frac{1}{NL}\sum_{k=0}^{\frac{NL}{8}-1}\Big(X_k + X_{k+\frac{NL}{8}} + X_{k+\frac{NL}{4}} + X_{k+\frac{3NL}{8}} + X_{k+\frac{NL}{2}} + X_{k+\frac{5NL}{8}} \\ &\quad + X_{k+\frac{3NL}{4}} + X_{k+\frac{7NL}{8}}\Big)\mathrm{W}_{\frac{NL}{8}}^{-ks} \end{aligned} \tag{3.9}$$

and, the rest $(NL/8)$-point IDFT output with $n_0 \in \{1, 2, \cdots, 7\}$ are given collectively as

$$x_{8s+n_0} = \frac{1}{NL}\sum_{k=0}^{\frac{NL}{8}-1}\left(\left(\sum_{q=0}^{7} X_{k+\frac{qNL}{8}}\mathrm{W}_8^{-qn_0}\right)\mathrm{W}_{NL}^{-kn_0}\right)\mathrm{W}_{\frac{NL}{8}}^{-ks}, \tag{3.10}$$

where $q = 0, 1, \cdots, 7$ and $s = 0, 1, \cdots, NL/8 - 1$. The flow graph of this radix-8-based algorithm is depicted in Fig. 3.2 with twiddle factors $\mathrm{W}_8^{-qn_0}$ being neglected.

It can be observed from (3.9) and (3.10) that for a specific $(NL/8)$-point IDFT, each input sample is a linear combination among eight $(NL/8)$-equispaced components of the zero-padded input data sequence. Again, due to the padded zeros at the end of the original data, only the first two elements in the linear combinations of (3.9) and (3.10) are nonzero and the rest six zero. Hence, for each of these eight $(NL/8)$-point IDFTs, the actual input sequence is $\{X_k + \mathrm{W}_8^{-n_0}X_{k+\frac{NL}{8}} | k = 0, 1, \cdots, NL/8-1\}$, $n_0 \in \{0, 1, \cdots, 7\}$, which is of length $N/2$.

Similar to the case that corresponds to the SLM scheme, phase sequences which help generating candidate sequences are multiplied with the original input sequences that feed into these $(NL/8)$-point IDFTs. As will be detailed later, a same phase sequence have to be multiplied by the original input sequences element-wise for all $(NL/8)$-point IDFTs to generate a specific candidate sequence and to correspond to a PTS scheme.

To begin with, we note that (3.10) can be alternatively rewritten as the following for

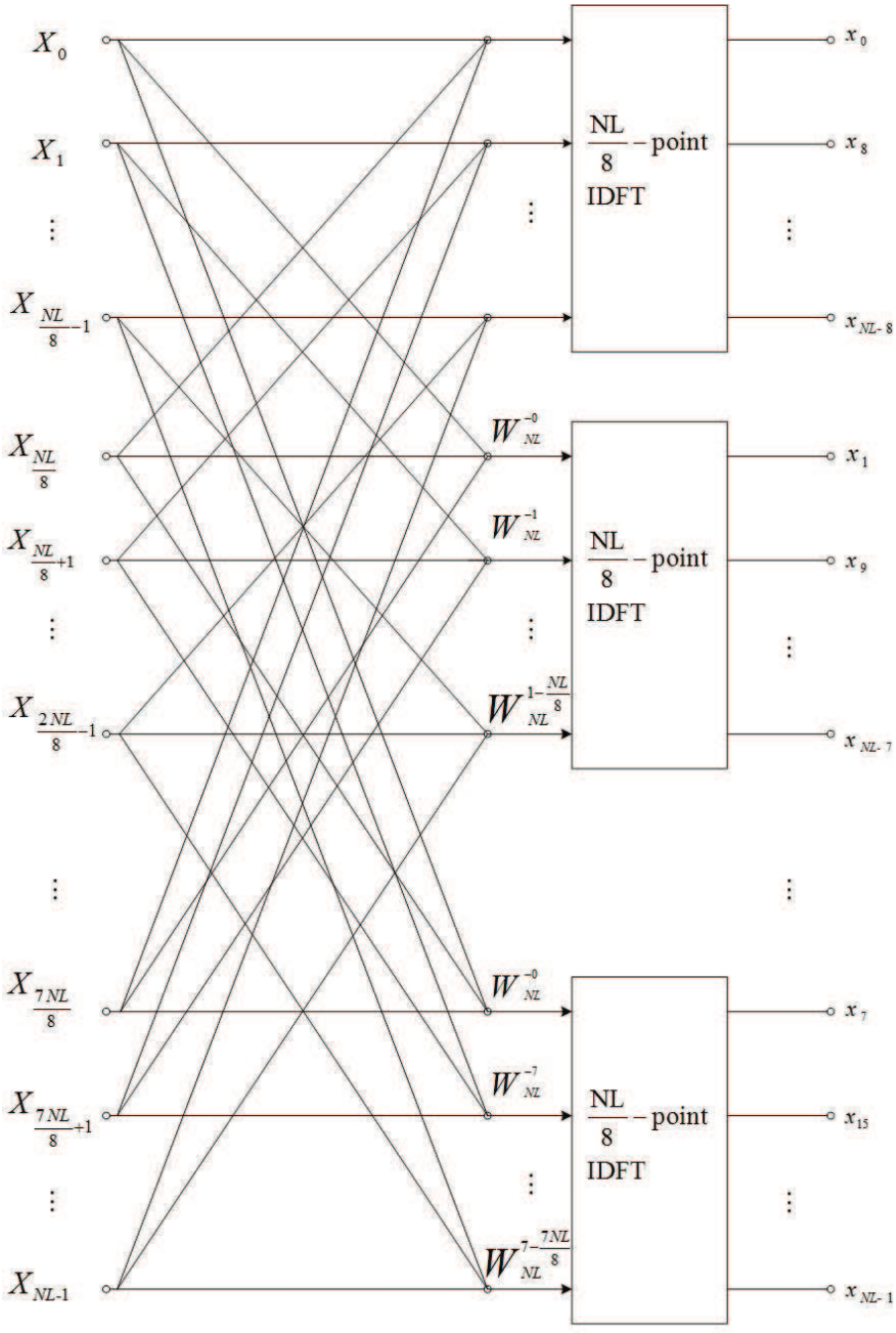

Figure 3.2: Flow graph of the radix-8 DIT of an NL-point IDFT computation into eight $(NL/8)$-point IDFTs.

$n_0 = 0, 1, \cdots, 7$:

$$x_{8s+n_0} = \sum_{k=0}^{\frac{NL}{8}-1} \left(\frac{1}{NL} \sum_{q=0}^{7} X_{k+\frac{qNL}{8}} \mathrm{W}_{NL}^{-(k+\frac{qNL}{8})(8s+n_0)} \right) \tag{3.11}$$

the sum of the NL-point IDFTs of $M = NL/8$ subblocks

$$\mathbf{X}_k = [\underbrace{0, \cdots, 0}_{k}, X_k, \underbrace{0, \cdots, 0}_{\frac{NL}{8}-1}, X_{k+\frac{NL}{8}}, 0, \cdots, 0, X_{k+\frac{7NL}{8}}, \underbrace{0, \cdots, 0}_{\frac{NL}{8}-k}] \tag{3.12}$$

where $k = 0, 1, \cdots, M-1$. Recall that the PTS scheme with M subblocks employed can be represented as (2.10). Therefore, it is possible to implement the corresponding PTS scheme via our proposal. Specifically, the implementation is given as

$$\begin{aligned} x'_{8s+n_0}(\mathbf{B}^{(u)}) &= \sum_{k=0}^{M-1} b_k^{(u)} \cdot IDFT\{\mathbf{X}_k\} \\ &= \frac{1}{NL} \sum_{k=0}^{\frac{NL}{8}-1} \left(\left(\sum_{q=0}^{7} X_{k+\frac{qNL}{8}} \mathrm{W}_8^{-qn_0} \right) \mathrm{W}_{NL}^{-kn_0} \right) b_k^{(u)} \mathrm{W}_{\frac{NL}{8}}^{-ks} \end{aligned} \tag{3.13}$$

where $\mathbf{B}^{(u)} = [b_0^{(u)}, b_1^{(u)}, \cdots, b_{M-1}^{(u)}]^T$, $s = 0, 1, \cdots, NL/8 - 1$, and $n_0 = 0, 1, \cdots, 7$. Obviously, just like the corresponding SLM scheme, the calculation in the outer brackets can be done beforehand and stored for the use by all phase sequences $\mathbf{B}^{(u)}$, where $u = 1, 2, \cdots, U$ and U is the number of candidate sequences. Since this calculation is performed only once for a specific OFDM symbol, a great amount of computation is saved with PAPR reduction performance maintained.

For the general case of $r > L$ ($L = 4$) where r is a multiple of 4, the mathematical expression of our radix-r decomposition is represented as

$$x_{rs+n_0} = \frac{1}{NL} \sum_{k=0}^{\frac{NL}{r}-1} \left(\left(\sum_{q=0}^{r-1} X_{k+\frac{qNL}{r}} \mathrm{W}_r^{-qn_0} \right) \mathrm{W}_{NL}^{-kn_0} \right) \mathrm{W}_{\frac{NL}{r}}^{-ks}, \tag{3.14}$$

where $q = 0, 1, \cdots, r-1$, $s = 0, 1, \cdots, NL/r - 1$, $n_0 = 1, 2, \cdots, r-1$. According to the analysis of case of radix-8 above, it is known that there are r/L components that are

nonzero and the rest zero in the inner summations because of the zero-padding. Therefore, we have $M = NL/r$ subblocks with each containing only r/L nonzero components. Analogous to the previous case, the corresponding PTS scheme can be implemented.

Again, finally, (NL/r)-point IDFTs are efficiently implemented by the radix-r' IFFT for r' if NL/r is a power of r'.

3.1.3 Proposed Stop Criterion

A stop criterion is proposal in this subsection to further reduce the computational complexity by dropping unnecessary calculations. Before introducing this criterion, two points have to be highlighted.

First, recall the definition of the PAPR of a signal

$$PAPR = \frac{\max\limits_{0 \le n < NL-1} |x_n|^2}{E\left[|x_n|^2\right]}, \tag{3.15}$$

where $x_n | n = 0, 1, \cdots, NL-1$, are time-domain samples and L is the factor of oversampling. The set of allowed phase factors is written as $P = \{e^{j2\pi l/W} | l = 0, 1, \cdots, W-1$ from which elements of $\mathbf{B}^{(u)}$ can choose, where W is the number of allowed phase factors (angles). It can be noticed that all allowed phase factors locate on the unit circle, i.e. their magnitudes are all 1. We can show that for all U candidate sequences $\mathbf{x}^{(u)}$ which are the IDFT of $\mathbf{X}^{(u)}$ derived via element-wise multiplication (3.7) or (3.13), their expected power $E\left[|x_n^{(u)}|^2\right]$ is a constant if elements of $\mathbf{B}^{(u)}$ are drawn from the polyphase set P. Therefore, we can focus only on the peak value of each candidate sequence (the numerator of (3.15)) instead of calculating (3.15) wholely when choosing the one with the lowest PAPR in our proposed algorithms.

Second, as discussed in the previous subsections, the basic structure in our proposed algorithms is the radix-r DIT IFFT algorithm which owns a particular character that can be utilized to reduce the amount of calculations. Besides, from Fig. 3.3, it can be noted that the original NL-point IDFT is decomposed into $r \times (NL/r)$-point IDFTs with linear combinations at the first stage and the output sequence of each (NL/r)-point

IDFT is a fraction of the length-NL oversampled time-domain samples. Therefore, the fact that in our proposed algorithms, these $r \times (NL/r)$-point IDFT can be computed *sequentially* enables us to early terminate the procedure for determining a candidate's PAPR immediately if its intermediate peak value already exceeds the minimum one calculated from the previous candidate sequences. In this way, needless calculations are avoided and thus the computational complexity decreased. In the following discussion, the detail of the proposed stop criterion is introduced.

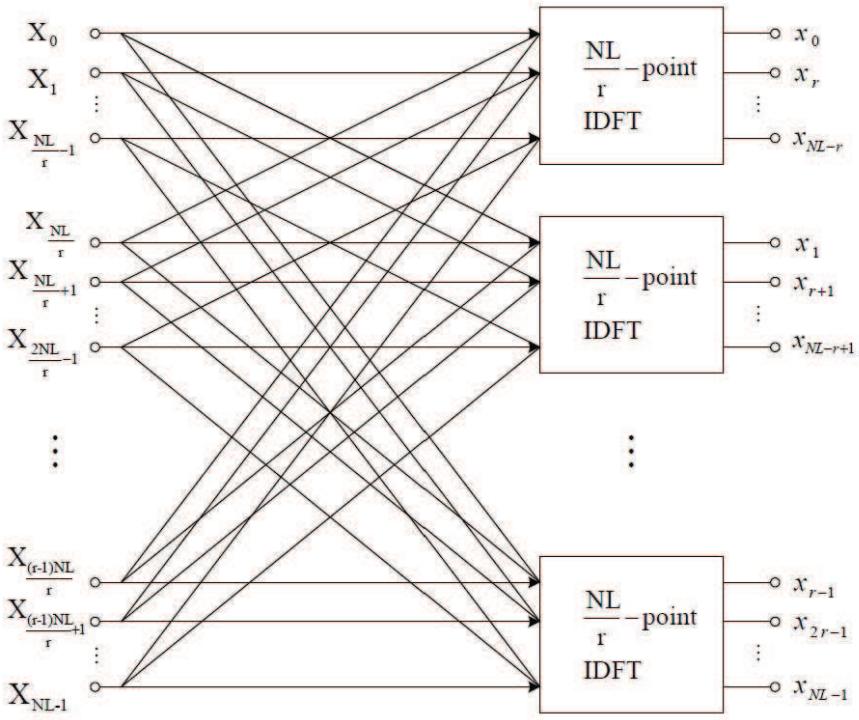

Figure 3.3: Flow graph of the radix-r DIT decomposition of an NL-point IDFT computation into $r \times (NL/r)$-point IDFT computations.

Our proposed stop criterion is executed by comparing and terminating. To launch this process, it is necessary to have a reference value for comparison. We take the corresponding SLM scheme with radix-4 at the first stage as an example and give some figures to illustrate the proposed stop criterion. Hence, in the beginning, the peak value of the candidate sequence without phase rotation $\mathbf{X}^{(1)} = \mathbf{X}$, i.e. the original sequence, is taken as the reference value P_{ref} to which $P_{i,j}$, denotes the peak value of the jth $(NL/4)$-

point IDFT output of the ith candidate sequence for $i = 2, 3, \cdots, U$ and $j = 1, 2, \cdots, 4$, is compared to.

We start from the second candidate sequence ($i = 2$), $NL/4$ time-domain samples are obtained after calculating the first $(NL/4)$-point IDFT. The peak value among these samples are found out and called $P_{2,1}$ as shown in the frame of Fig. 3.4. Then,

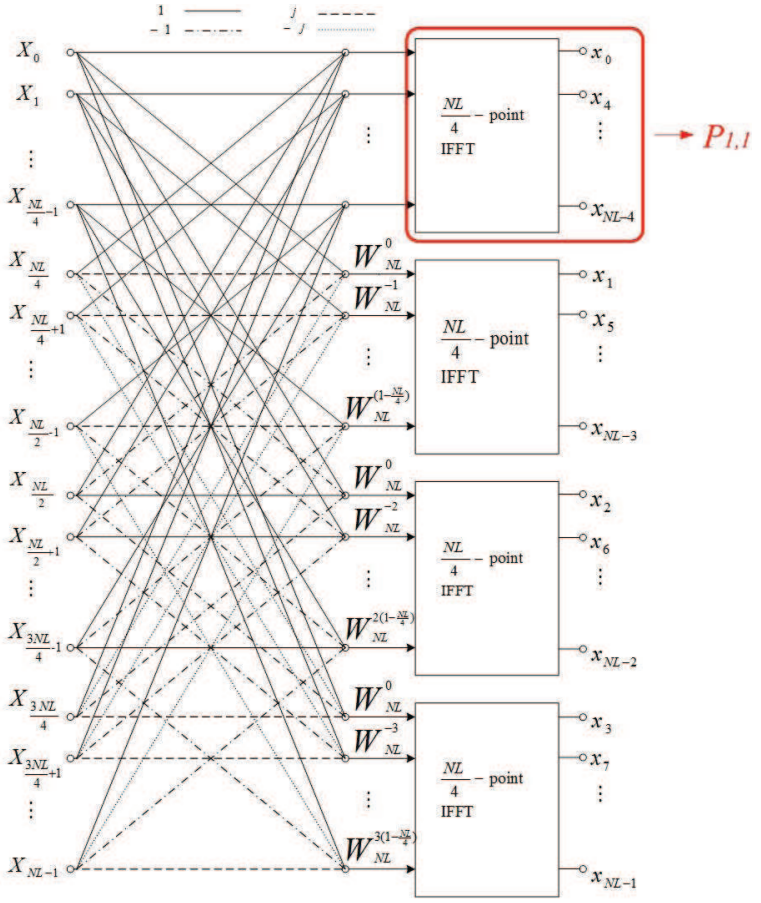

Figure 3.4: Illustration of the proposed stop criterion (I).

$P_{2,1}$ is compared to the reference peak value P_{ref}. If $P_{2,1} \geq P_{ref}$, it can be figured out from (3.15) that the PAPR value of the second candidate sequence, generated by the second phase sequence, must be larger than that of the time-domain samples of the original input data block. It is obvious that the second candidate sequence cannot achieve better performance of PAPR reduction, so the process to generate this candidate

sequence is terminated and the rest operations are dropped. Otherwise, the PAPR of this candidate sequence may be lower than that of the original input data, so the peak value of the second $(NL/4)$-point IDFT output samples $P_{2,2}$ is necessary to be computed and compared with P_{ref} as depicted in Fig. 3.5.

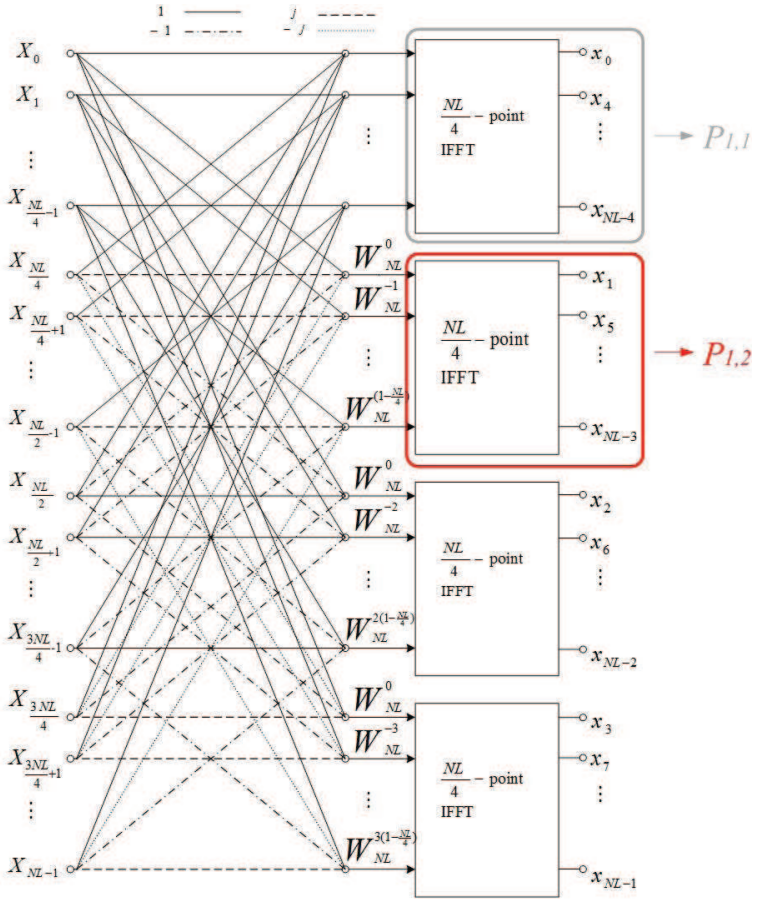

Figure 3.5: Illustration of the proposed stop criterion (II).

As the same account mentioned above, comparing $P_{2,2}$ with P_{ref} is required to decide whether this candidate sequence can achieve better PAPR reduction performance or not. If $P_{2,2} \geq P_{ref}$, we terminate the current process immediately, drop the rest processes to generate this candidate sequence, and move on to the computation of the next candidate sequence. Otherwise, it is requested to calculate the peak value of the third $(NL/4)$-point IDFT output $P_{2,3}$ and so on. Finally, if $P_{2,4}$ is still smaller than P_{ref}, it can be

Table 3.1: The Proposed Algorithm

$\mathbf{X}^{(1)} = [X_0, X_1, \cdots, X_{N-1}]$

$\mathbf{x} = IDFT\{\mathbf{X}\}$

$P_{ref} = \max(|\mathbf{x}|^2)$

`For` $u = 2$ `to` U

compute $P_{u,1}$;

let $s = 2$;

`while((`$P_{u,j} < P_{ref}, j < s$`)&&(`$s \leq r$`))` `do`

compute $P_{u,s}$;

s++;

`end`

`if((`$s - 1 = r$`)&&(`$P_{u,r} < P_{ref}$`))`

update $P_{ref} = \max(P_{u,j} | j = 1, \ldots, r)$;

`end`

`end`

concluded that the PAPR of this candidate sequence is lower than that of the original input data block and P_{ref} is updated by the largest among $P_{2,j}, j = 1, 2, 3, 4$, and PAPR of the second candidate sequence is recorded.

In general, based on the proposed stop criterion, r (NL/r)-point IDFTs are executed sequentially so that we can derive the peak value a part of the time-domain samples at a time. Therefore, the process of generating candidate sequence can be terminated once the peak value of a part of this candidate sequence already exceeds the reference value P_{ref}. The complete procedure is summarized in Table (3.1). As we can see that unnecessary computations are neglected to lower the amount of computations. Accordingly, the computational complexity is reduced by employing the proposed stop criterion.

3.2 Performance Analysis and Comparison

3.2.1 Analysis of Computational Complexity

Compared to the conventional SLM and PTS schemes, our proposed radix-r DIT IFFT algorithm can reduce the computational complexity effectively on account of two reasons. First, each phase sequence is multiplied with the input of the $r \times (NL/r)$-point IDFTs corresponding to the original data block $\mathbf{X}$, so the computation result of the first stage for a given OFDM symbol can be preserved and used for all U phase sequences. In other words, the results of stage one for a specific OFDM symbol have to be calculated only once so that the computational complexity decreases. Second, by checking our proposed stop criterion sequentially, process of generating a particular candidate sequence can be terminated immediately once we are certain that this candidate sequence fails to reach a better PAPR reduction performance.

In order to compare the computational complexity of the proposed schemes and conventional schemes, we define the computational complexity ratio as

$$R = \frac{\text{Complexity of proposed scheme}}{\text{Complexity of conventional scheme}} \times 100\%.$$

The comparison of computational complexity is shown in Table 3.2 and 3.3, and the computational complexity ratio of various schemes is also given in Table 3.4 and 3.5. Note that the worst case complexity is adopted here to measure the performance of the proposal algorithms. As for the conventional PTS scheme, the number of subblocks (M) is replaced by NL/r, which is equivalent to the number of subblocks for our proposed PTS scheme, and r is the value of radix-r used at the first stage in our proposal.

3.2.2 Simulation Results

Simulations are performed to evaluate the PAPR reduction performance of the proposed corresponding SLM and PTS schemes. Here, the input data are 16-QAM

Table 3.2: Computational Complexity of Various Schemes (I)

	Number of complex multiplications
Conventional SLM scheme	$U\left(\frac{NL}{2}\cdot\log_2 NL\right)$
Proposed SLM scheme	$NL\left(1+\frac{U}{2}\cdot\log_2 N\right)$
Conventional PTS scheme	$\frac{(NL)^2}{2r}\cdot\log_2 NL$
Proposed PTS scheme	$\frac{NL}{2}\left(\log_2 r+U\cdot\log_2\frac{NL}{r}\right)$

Table 3.3: Computational Complexity of Various Schemes (II)

	Number of complex additions
Conventional SLM scheme	$U\left(NL\cdot\log_2 NL\right)$
Proposed SLM scheme	$NL\left(1+U\cdot\log_2 N\right)$
Conventional PTS scheme	$\frac{(NL)^2}{r}\cdot\log_2 NL$
Proposed PTS scheme	$NL\left(\log_2 r+U\cdot\log_2\frac{NL}{r}-1\right)$

modulated and the OFDM system contains $N = 256$ subcarriers. To estimate the PAPR, the OFDM symbol is oversampled by a factor of $L = 4$.

Figure 3.6 compares the PAPR performance of the proposed SLM scheme with proposed stop criterion and that of the conventional SLM scheme. It is seen that for a given number of candidate sequences (U), the PAPR reduction performance of the proposed, which is of lower computational complexity is identical to that of the conventional one.

The PAPR reduction performance of the proposed and the conventional PTS scheme with number of candidate sequences set to be $U = 8$ is shown in Fig. 3.7. Again, noted that the proposed PTS scheme can achieve the same performance as the conventional one for a given number of subblocks (M) while having a lower complexity.

Table 3.4: Computational Complexity Ratio of the Proposed SLM Scheme with $N = 256$

	R_{mul} (%)	R_{add} (%)
$U = 8$	82.5	81.25
$U = 32$	80.63	80.31

Table 3.5: Computational Complexity Ratio of the Proposed PTS Schemes with $N = 256$ and $U = 8$.

	$r = 32(M = 32)$		$r = 128(M = 8)$		$r = 256(M = 4)$	
	R_{mul} (%)	R_{add} (%)	R_{mul} (%)	R_{add} (%)	R_{mul} (%)	R_{add} (%)
$U = 8$	14.06	13.75	38.75	37.50	60	57.50

3.3 Proposed Algorithm with Conversion Vectors

In general, the SLM and PTS schemes can provide significant PAPR reduction performance, but each of them may require a high computational load due to the need of a bank of IDFTs. Therefore, we are interest in the methods which reduce the computational complexity of both SLM and PTS schemes.

3.3.1 Brief introduction for LWW Scheme

It has been introduced in [12] that the IDFT operations were substituted for conversion vectors which are specified in the form of perfect sequences so that the corresponding phase sequences all have the same magnitude to avoid the degradation of BER performance. In [12], candidate sequences can generated by applying an NL-point circular convolution of the time-domain with conversion vector which are composite of base vectors. To reduce the computational complexity of the conversion process, the conversion vectors whose length are all NL have to comply with some constrains. Accordingly, three classes of conversion vectors were proposed in [12], and three novel low-complexity SLM schemes we called LWW Schemes were implemented with these three classes conversion vectors.

According to the discrete Fourier transform (DFT) properties, if a time-domain signal x_n is time-shifted by an amount of Δ (resulting in a signal $x_{n-\Delta}$), its frequency-domain representation is simply multiplied by a phase shift term of $\frac{-j2\pi k\Delta}{N}$. Besides, circular convolution in time-domain becomes multiplication in frequency-domain. Therefore, a candidate sequence can be generated by performing a circular convolution of the IDFT

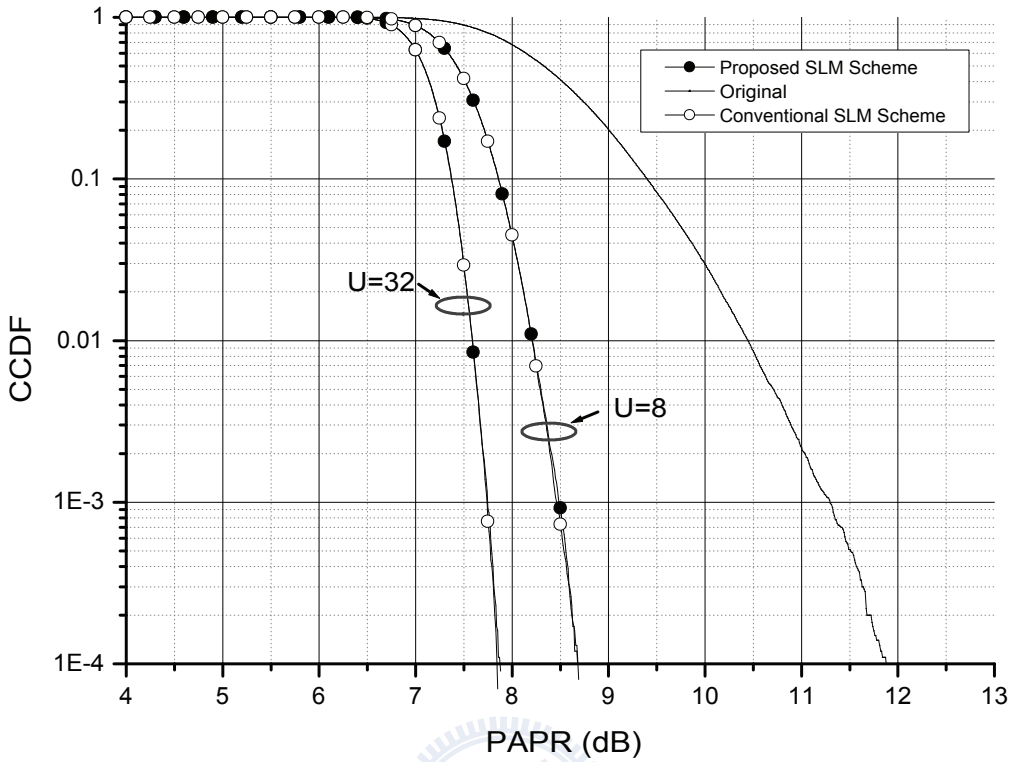

Figure 3.6: Comparison of PAPR performance of Proposed SLM Scheme and conventional SLM Scheme.

of input data block with these three classes conversion vectors, and various numbers of right cyclic shift of base vectors can obtained a number of candidate sequences. Figure 3.8 illustrates the architecture of LWW Scheme I where $\mathbf{G}_{a1}$, $\mathbf{G}_{a2}$, $\mathbf{G}_{b1}$ and $\mathbf{G}_{b2}$ are the base vectors of conversion vectors $\mathbf{G}_a$ and $\mathbf{G}_b$, respectively.

From Fig. 3.8, it can be noted that only one NL-point IDFT is required to generate a number of candidate sequences by performing circular convolution and cyclic shifts, the computational complexity can be reduced significantly for LWW Schemes at the cost of PAPR reduction performance.

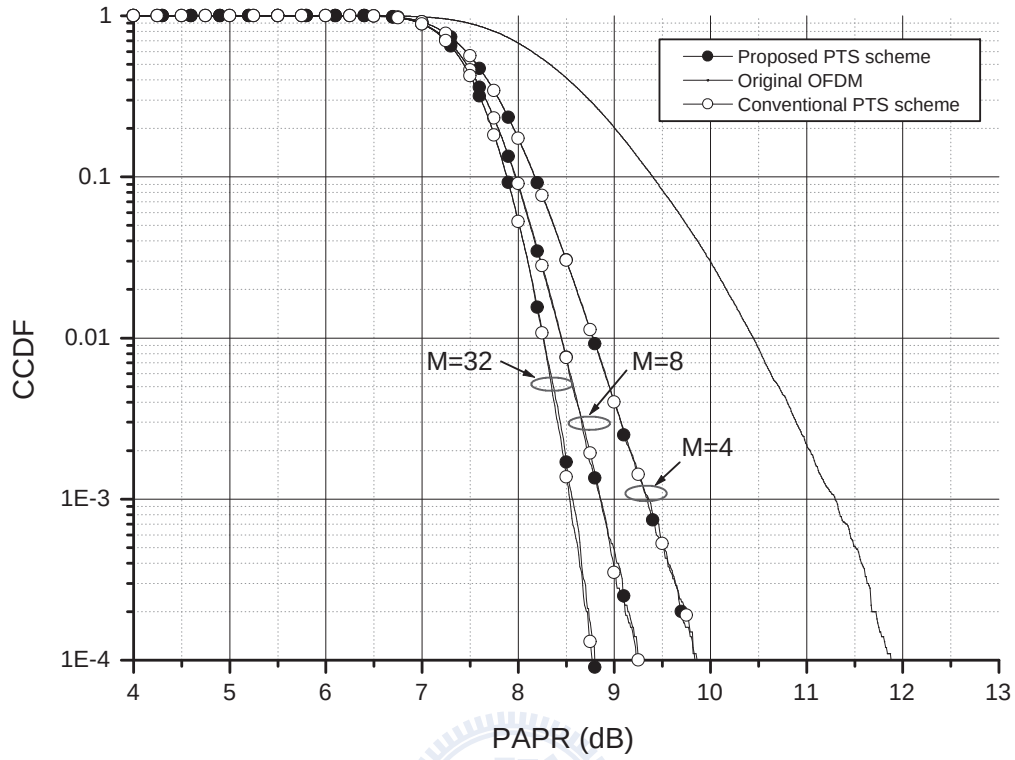

Figure 3.7: Comparison of PAPR performance of Proposed PTS Scheme and conventional PTS Scheme.

3.3.2 Modified LWW Scheme with Proposed Stop Criterion

To reduce the computational complexity of our proposal further, LWW Scheme is considered with some modifications. First, the NL-point IDFT is replaced by our proposed algorithm which has been introduced in previous section. The second modification is about the length of base vectors which is length-NL in LWW Scheme. To adapt the conversion vectors to our schemes, the length of base vectors have to be changed to NL/r. Figure 3.9 shows the architecture of convolution structure in which $\mathbf{H}_{a1}$, $\mathbf{H}_{a2}$, $\mathbf{H}_{b1}$ and $\mathbf{H}_{b2}$ denote the base vectors after length modification (i.e. length-(NL/r)). Therefore, the complete structure of our proposed scheme with conversion vectors is presented in Fig 3.10. Similarly, the computation of $r \times (NL/r)$-point IDFTs are computed once for

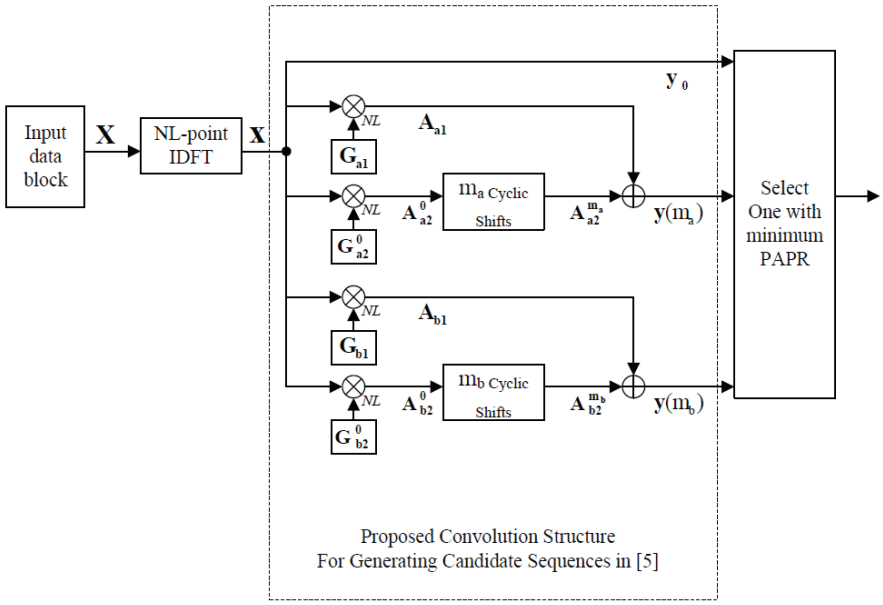

Figure 3.8: Architecture of L&W Scheme I.

a given OFDM symbol, and a number of candidate sequences are generated by applying circular convolution of base vectors with the out samples of $r \times (NL/r)$-point IDFTs.

Furthermore, since we can derive the length-(NL/r) output sequence which is a fraction of certain length-NL candidate sequence sequentially, the proposed stop criterion can also be considered in this modified scheme to lower the computational complexity.

3.3.3 Analysis of Computational Complexity

For all $r \times (NL/r)$-point IDFTs, each of them only needs to be performed once for a given OFDM symbol when length-modified LWW Scheme is combined to our proposed algorithm. Therefore, our proposed schemes with length-modified conversion vectors result in lower computational complexity compares with conventional SLM scheme, conventional PTS scheme, and our proposed schemes in preceding section.

There are three LWW Schemes proposed in [12]. The scheme introduced in previous subsection is LWW Scheme I. LW Scheme II is constructed by combining LWW Scheme I and the conventional SLM scheme to enhance the PAPR reduction performance. Two

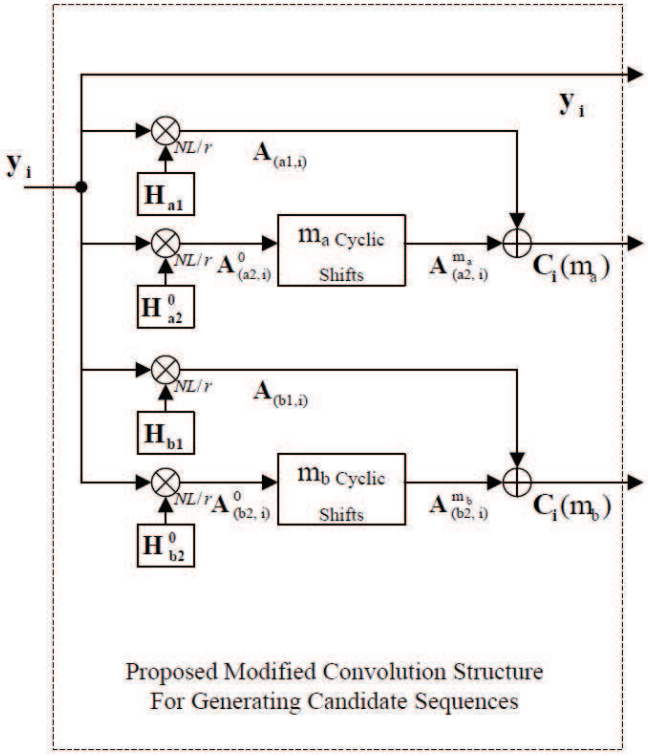

Figure 3.9: Architecture of modified convolution structure for generating candidate sequences.

parallel IDFTs are required and a random phase sequence is adopted before the second IDFT operation. This random phase sequence can increase the diversity of candidate sequences, resulting in a better performance of PAPR reduction, but higher computational complexity due to one more IDFT operation. LWW Scheme III has the same structure as LWW Scheme I while the third class conversion vectors proposed in [12] is used.

It can be noticed that for LWW Scheme I and LWW Scheme III, the corresponding schemes based on our proposed algorithm with length-modified conversion vectors can achieve the same number of complex multiplications. The corresponding Scheme II in our proposed algorithm requires less complexity than LWW Scheme II since the computation of the first stage only needs to compute once and reuses for two sets of $r \times (NL/r)$-point IDFTs. Besides, our proposed corresponding schemes can achieve less number of

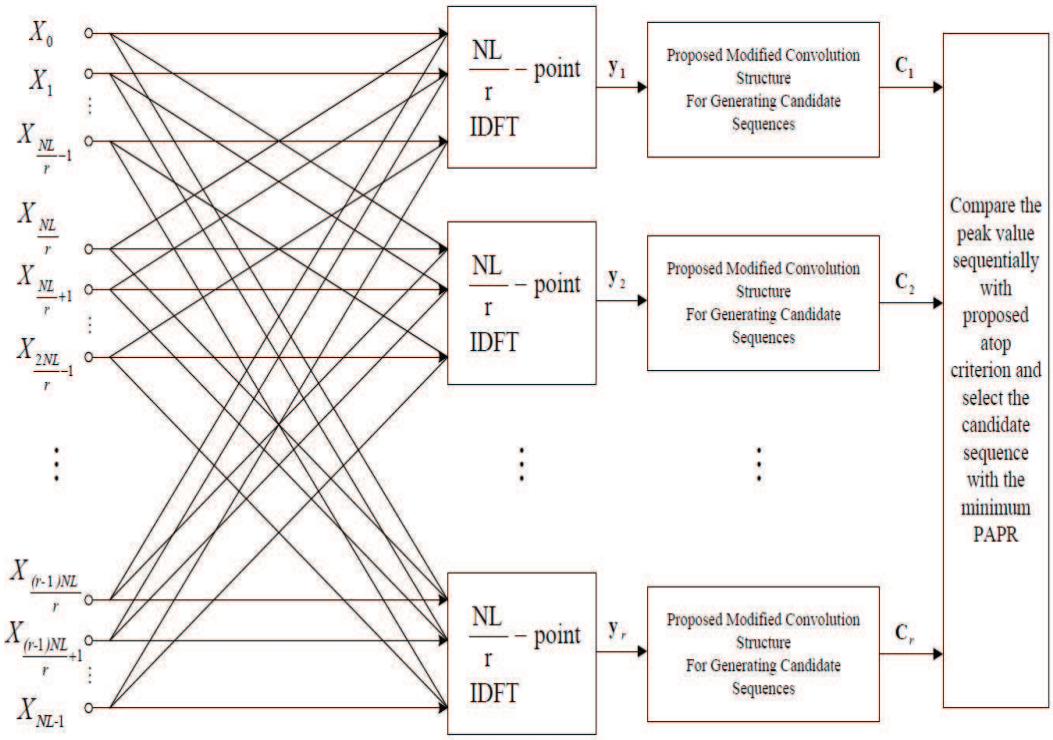

Figure 3.10: Architecture of our proposed scheme with conversion vectors.

complex additions due to the use of L-oversampling.

Table 3.6 and 3.7 present the computational complexity of various SLM schemes, including the conventional SLM scheme, LWW Schemes, and corresponding Schemes based on our proposed algorithm. However, only SLM scheme can be implemented in LWW Schemes so that Table 3.8 and 3.9, which are the comparison of various PTS schemes, just compare the conventional PTS scheme and corresponding scheme based on our proposed algorithm. It is worth noting that the worst case of our schemes is considered here while the computational complexity can be reduced further if the proposed stop criterion is considered.

In addition, computational complexity ratio for the conventional SLM and PTS schemes and our corresponding schemes is given in table 3.10 and 3.11.

Table 3.6: Computational complexity of various SLM schemes (I)

	Number of complex multiplications
Conventional SLM Scheme	$U\left(\frac{NL}{2} \cdot \log_2 NL\right)$
LWW Scheme I	$\frac{NL}{2} \cdot \log_2 NL$
LWW Scheme II	$NL \cdot \log_2 NL$
LWW Scheme III	$\frac{NL}{2} \cdot \log_2 NL$
Proposed modified Scheme I for SLM	$\frac{NL}{2} \cdot \log_2 NL$
Proposed modified Scheme II for SLM	$NL(1 + \log_2 N)$
Proposed modified Scheme III for SLM	$\frac{NL}{2} \cdot \log_2 NL$

Table 3.7: Computational complexity of various SLM schemes (II)

	Number of complex additions
Conventional SLM Scheme	$U(NL \cdot \log_2 NL)$
LWW Scheme I	$NL(\log_2 NL + U + 7)$
LWW Scheme II	$NL(2 \cdot \log_2 NL + U + 14)$
LWW Scheme III	$NL(\log_2 NL + 3U)$
Proposed modified Scheme I for SLM	$NL(\log_2 N + U + 8)$
Proposed modified Scheme II for SLM	$NL(2 \cdot \log_2 N + U + 15)$
Proposed modified Scheme III for SLM	$NL(\log_2 N + 3U + 1)$

3.3.4 Simulation Results

In this section, we investigate the PAPR performance of various PAPR reduction schemes when 16-QAM is employed with $N = 256$. Besides, $L = 4$ which is the factor of oversampling is considered.

Fig. 3.11 compares the PAPR reduction performance of our Proposed Modified

Table 3.8: Computational complexity of various PTS schemes (I)

	Number of complex multiplications
Conventional PTS Scheme	$\frac{(NL)^2}{2r} \cdot \log_2 NL$
Proposed modified Scheme I for PTS	$\frac{NL}{2} \cdot \log_2 NL$
Proposed modified Scheme II for PTS	$\frac{NL}{2} \log_2 r + NL \cdot \log_2 \frac{NL}{r}$
Proposed modified Scheme III for PTS	$\frac{NL}{2} \cdot \log_2 NL$

Table 3.9: Computational complexity of various PTS schemes (II)

	Number of complex additions
Conventional PTS Scheme	$\frac{(NL)^2}{r} \cdot \log_2 NL$
Proposed modified Scheme I for PTS	$NL(\log_2 NL + U + 6)$
Proposed modified Scheme II for PTS	$NL\left(\log_2 r + 2 \cdot \log_2 \frac{NL}{r} + U + 13\right)$
Proposed modified Scheme III for PTS	$NL(\log_2 NL + 3U - 1)$

Table 3.10: Computational complexity ratio for Proposed SLM Schemes over the conventional SLM scheme with $N = 256$.

	Proposed Scheme I		Proposed Scheme II		Proposed Scheme III	
	R_{mul} (%)	R_{add} (%)	R_{mul} (%)	R_{add} (%)	R_{mul} (%)	R_{add} (%)
$U = 8$	12.50	30.00	22.50	48.75	12.50	41.25
$U = 32$	3.13	15.00	5.63	19.69	3.13	32.81

Schemes I and II, LWW Scheme I and II, and conventional SLM schemes. It is seen that for a given number of candidate sequences (U), the PAPR reduction performance of both Proposed Modified Scheme I and II is similar to that of LWW Scheme I and II. From a detailed inspection, the performance degradation of Proposed Modified Scheme I and II relative to that of conventional SLM scheme are 0.4 and 0.16 dB, respectively for $U = 32$ and CCDF of of 10^{-4}. As expected, PAPR performance of Proposed Modified Scheme II is better that that of Proposed Modified scheme I for an extra IDFT operation.

Fig. 3.12 shows the PAPR reduction performance of our Proposed Modified Scheme III, LWW Scheme III and conventional SLM scheme. Note that our Proposed Modified Scheme III can achieve similar performance as LWW Scheme III, and the maximum performance loss of Proposed Modified Scheme III relative to the conventional SLM scheme is 0.12 dB for $U = 32$ and CCDF of 10^{-4}.

As mentioned in previous subsection, LWW Schemes are just applied to SLM scheme, so comparison of PTS schemes just includes our Proposed Modified Schemes and the conventional PTS scheme. In Fig. 3.13, PAPR reduction performance of Proposed Modified Schemes I and II, and conventional PTS scheme is presented with $U = 8$. It

Table 3.11: Computational complexity ratio for Proposed PTS Schemes over the conventional PTS scheme with $N = 256$ and $U = 8$.

	Proposed Scheme I		Proposed Scheme II		Proposed Scheme III	
	R_{mul} (%)	R_{add} (%)	R_{mul} (%)	R_{add} (%)	R_{mul} (%)	R_{add} (%)
$r = 32(M = 32)$	3.13	7.50	4.69	11.25	3.13	10.31
$r = 128(M = 8)$	12.50	30.00	16.25	42.50	12.50	41.25
$r = 256(M = 4)$	25.00	60.00	30.00	82.50	25.00	82.50

can be noted that for a given number of subblocks (M), PAPR performances of Proposed Modified Scheme I and II are poorer than that of conventional PTS scheme. However, lower computational complexity of Proposed Modified schemes is provided.

Figure 3.14 illustrates the PAPR performance of Proposed Modified Scheme III and conventional PTS scheme with $U = 8$. For $M = 4$, two schemes provide almost the same performance. Although there are slight degradation of PAPR reduction performance for $M = 8$ and $M = 32$, less computational complexity is achieved for Proposed Modified Scheme III as shown in preceding section. It is shown that the performance loss of Proposed Modified Scheme III relative to the conventional PTS scheme is 0.12 dB for $M = 32$ and CCDF of 10^{-4}.

3.4 Transform Decomposition

The transform decomposition (TD) [14], a mixture of a Cooley-Tukey FFT and a computational structure similar to Goertzel's algorithm [15], has been introduced for computing only a subset of output points. Below, a mathematical derivation of TD for input with few nonzero point is given.

The discrete Fourier transform (DFT) is defined as

$$X_k = \sum_{n=0}^{N-1} x_n \mathrm{W}_N^{nk}, \quad k = 0, 1, \cdots, N-1. \tag{3.16}$$

Assume that there are L nonzero inputs and there exist a P which is the nearest power two integer larger than L such that P divides N and define $Q = N/P$. The index n and

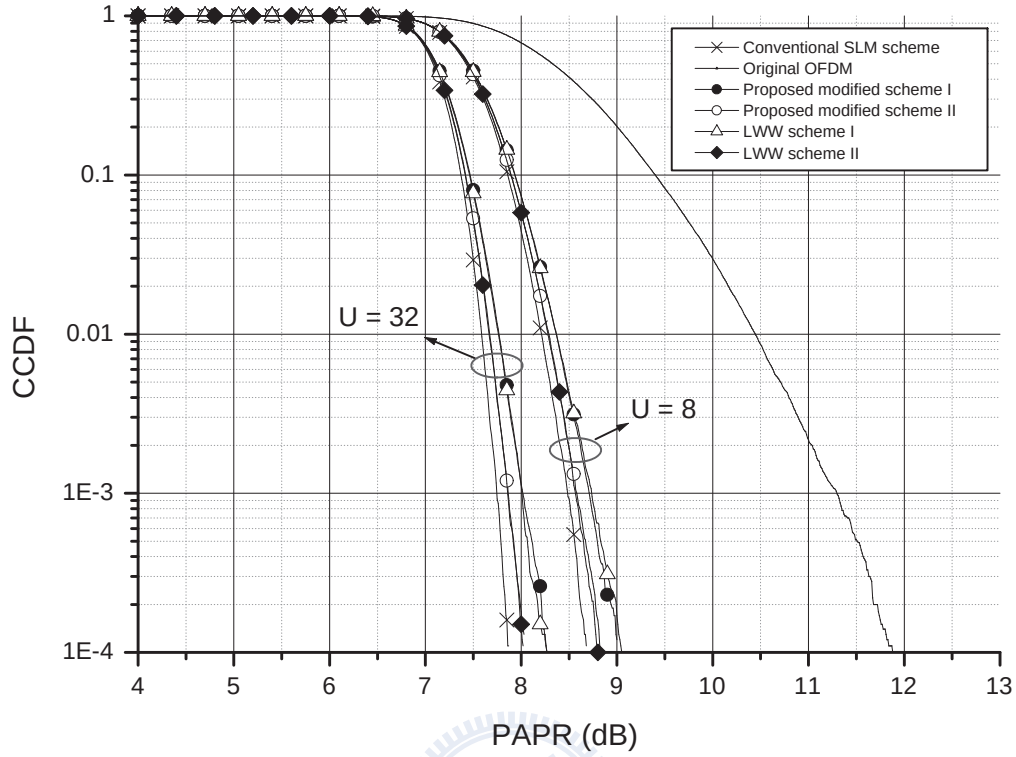

Figure 3.11: Comparison of PAPR reduction performance of the proposed modified schemes I and II, LWW schemes I and II, and conventional SLM schemes.

k can be written as

$$n = Qn_1 + n_2 \qquad \begin{matrix} n_1 = 0, 1, \cdots, P-1 \\ n_2 = 0, 1, \cdots, Q-1 \end{matrix} \tag{3.17}$$

and

$$k = k_1 + Qk_2 \qquad \begin{matrix} k_1 = 0, 1, \cdots, Q-1 \\ k_2 = 0, 1, \cdots, P-1. \end{matrix} \tag{3.18}$$

Using the variable substitution with (3.17) and (3.18), (3.16) can be rewritten as

$$\begin{aligned} X_{k_1+Qk_2} &= \sum_{n_2=0}^{P-1} \sum_{n_1=0}^{Q-1} x_{Pn_1+n_2} \mathrm{W}_N^{(Pn_1+n_2)(k_1+Qk_2)} \\ &= \sum_{n_2=0}^{P-1} \left(\sum_{n_1=0}^{Q-1} x_{Pn_1+n_2} \mathrm{W}_N^{(Pn_1+n_2)k_1} \right) \mathrm{W}_P^{n_2 k_2}. \end{aligned} \tag{3.19}$$

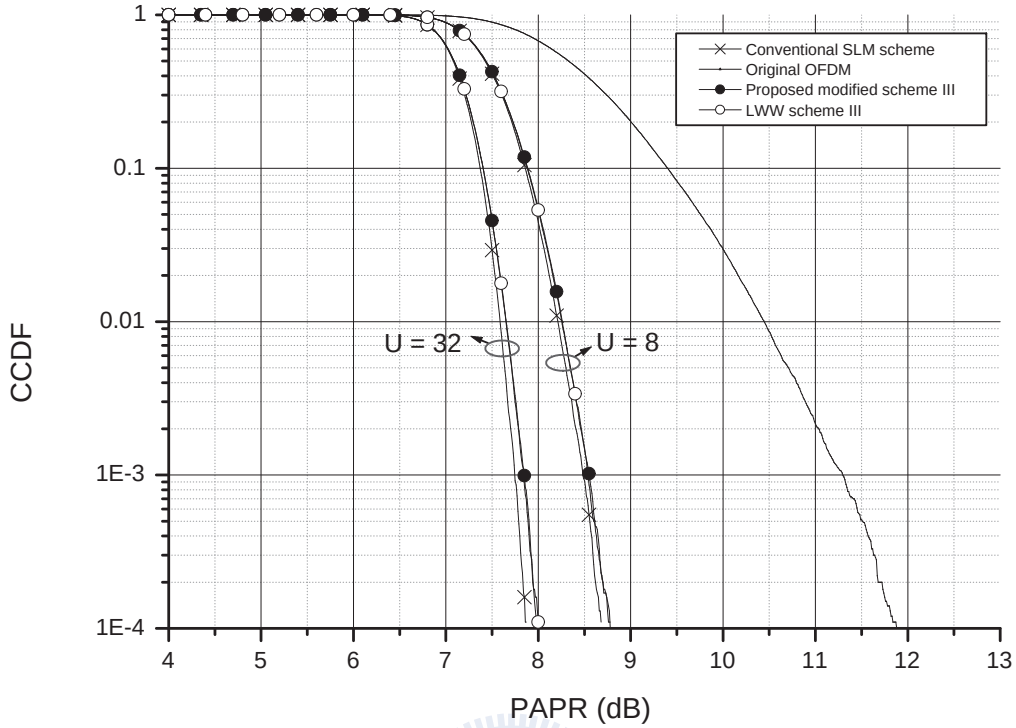

Figure 3.12: Comparison of PAPR reduction performance of the proposed modified scheme III, LWW scheme III, and conventional SLM scheme.

We can rewritten (3.19) as

$$X_{k_2}^{k_1} = \sum_{n_2=0}^{P-1} x_{n_2}^{k_1} \mathrm{W}_P^{n_2 k_2} \qquad \begin{matrix} k_1 = 0, 1, \cdots, Q-1 \\ k_2 = 0, 1, \cdots, P-1 \end{matrix} \tag{3.20}$$

where $X_{k_2}^{k_1} = X_{k_1+Qk_2}$ and

$$x_{n_2}^{k_1} = \sum_{n_1=0}^{Q-1} x_{Pn_1+n_2} \mathrm{W}_N^{k_1(Pn_1+n_2)}. \tag{3.21}$$

For a given k_1, (3.20) can be viewed as a P-point DFT and it can be computed efficiently using a FFT algorithm. As the k_1 range form 0 to $Q-1$, there are Q P-point DFT operations. For each P-point DFT, we need to acquire $x_{n_2}^{k_1}$ by using (3.21). Since there are L nonzero input points, the multiplications used by (3.21) are L at a given k_1 when n_2 traverses from 0 to $P-1$. Accordingly, the TD is a method for few

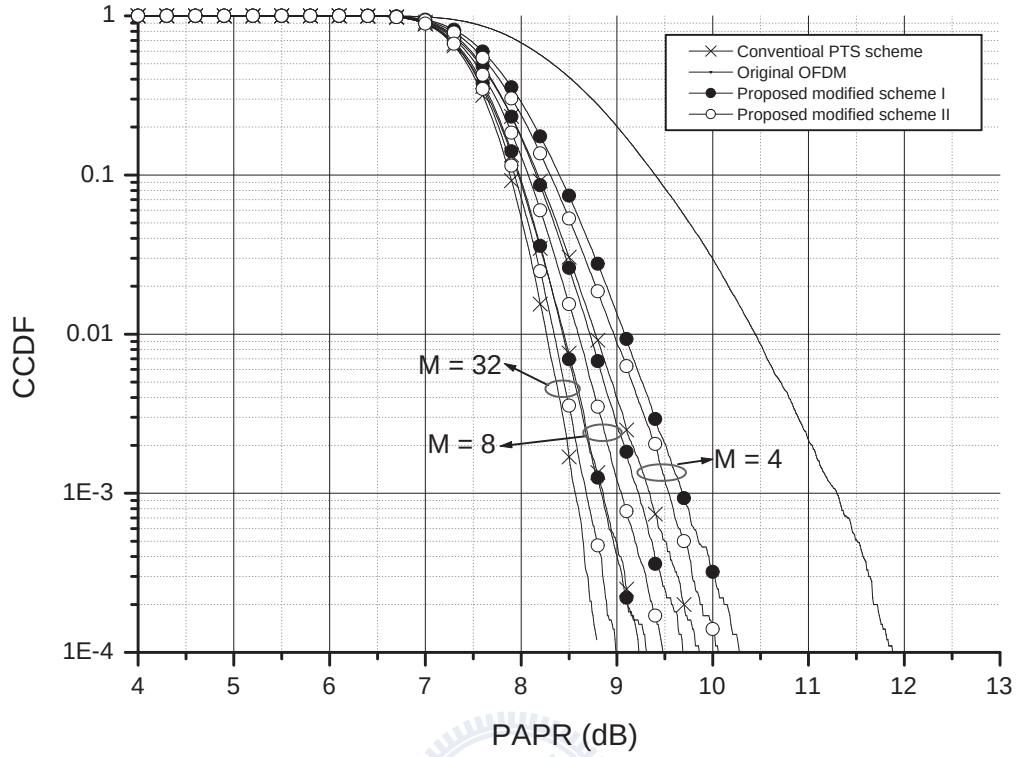

Figure 3.13: Comparison of PAPR reduction performance of the proposed modified schemes I and II, and the conventional PTS scheme.

nonzero elements of input data so that the computational complexity decreases. We can conclude that for TD, it decomposes an original N-point DFT into Q P-point DFT by using (3.21) for stage one and (3.20) for stage two. It can be noticed that the structure of TD is similar to that of our proposed algorithm.

For PAPR reduction method, TD method can be applied due to the execution of L-oversampling which combined length-N input data and $(L-1)N$ zeros consequently to form the exact input sequence for NL-point IDFT. Besides, we can find out the computational complexity of TD and our proposed algorithm are the same if only a candidate sequence is generated.

Since the phase sequences are applied to the input sequence of IDFT when TD

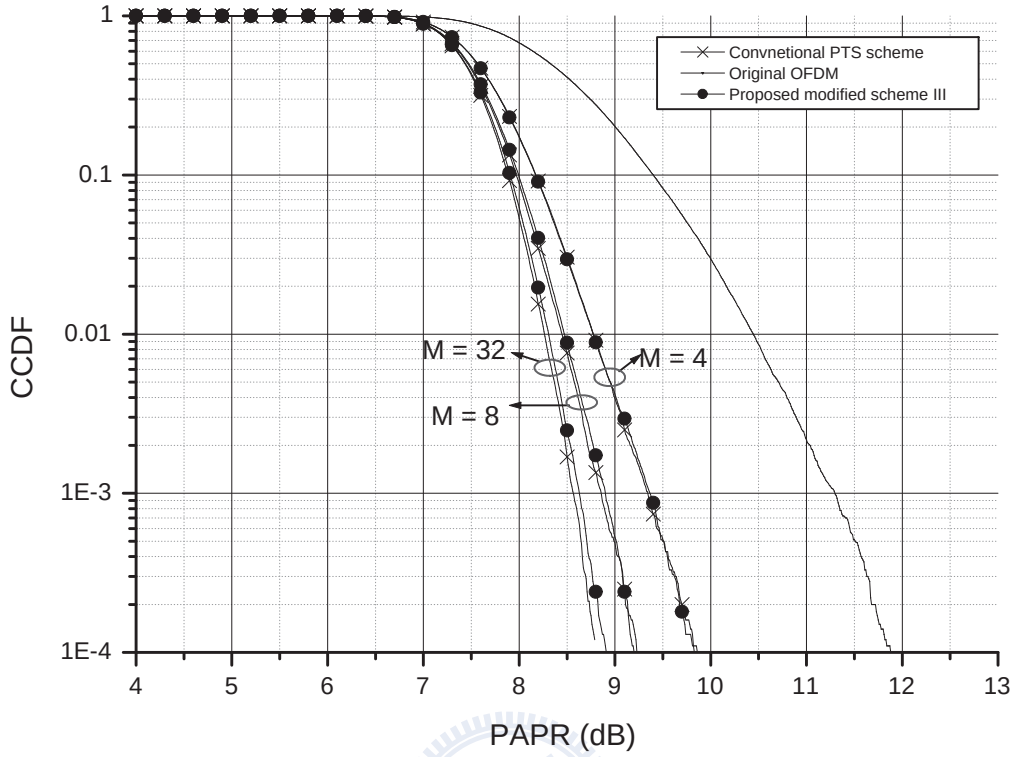

Figure 3.14: Comparison of PAPR reduction performance of the proposed modified scheme III and the conventional PTS scheme.

method is applied, a complete computation of TD method is required to generate a candidate sequence. However, in our proposed algorithm, for a given OFDM symbol, the computation of the first stage is calculated once and the computation result can be reused for remaining phase sequences since the phase sequences are applied at the end of the first stage.

Chapter 4

IDFT architecture aware PAPR reduction schemes II

4.1 Related work

As mentioned in the pervious chapter, one of the drawbacks of SLM and PTS schemes is the high computational complexity for the requirement of multiple IFFT operations. This issue has been resolved in [16], which will be refer to as the G&G SLM scheme from now on, by using the product of intermediate sequences within an IDFT and some phase factors, with DIF/DIT IFFT being adopted.

In this chapter, we introduce new SLM and PTS schemes for PAPR reduction with low computational complexity. The proposed schemes transform an input data block into a set of candidate sequences by carefully multiplying the phase sequences with intermediate sequences which are within an NL-point IDFT at different stages. The main difference between our scheme and G&G SLM scheme is that we add the phase in the intermediate stage suitably such that the generated sequence in frequency-domain is equivalent to the product of the data sequence and phase sequence counterpart, whose elements locate on the unite circle. With this property, we can show that the BER performance is not degraded while the computational complexity is reduced by our scheme.

4.2 Proposed New SLM and PTS Schemes

As mentioned in the previous chapter, the values of r for radix-r at stage 1 correspond our proposal to SLM and PTS schemes. Here, with such r determined and fixed, we propose *new* SLM and PTS schemes by investigating the decomposition of later stages.

4.2.1 Scheme Description

To introduce the proposed scheme, we first define some notations we will use in the rest of this chapter. As we consider the ηth IDFT of stage v, the input data and (frequency) indices for stage v are denoted by $\mathbf{X}^{(v,\eta)}$ and $k^{(v)}$, respectively. Similarly, $\mathbf{x}^{(v,\eta)}$ and $n^{(v)}$ are the output and (time) indices, respectively. Hence, the ηth intermediate (NL/r^{v-1})-point IDFT outputs at stage v are given by

$$x^{(v,\eta)}_{rn^{(v)}+n_0} = \frac{1}{r}\left(\sum_{q=0}^{r-1} X^{(v,\eta)}_{k^{(v)}+\frac{NL}{r^v}q} \cdot \mathrm{W}_r^{-qn_0}\right)\mathrm{W}^{-k^{(v)}n_0}_{NL/r^{v-1}} \tag{4.1}$$

where $k^{(v)} = 0, 1, \cdots, NL/r^v - 1$, $n^{(v)} = 0, 1, \cdots, NL/r^v - 1$, and $\eta = 1, 2, \cdots, r^{v-1}$.

As mentioned in Section 3.1, different values of r selected at the first stage for DIT IFFT result in distinct SLM or PTS schemes. For instance, if $r = 4$ is used in the first stage, it forms the SLM. For $r > 4$ and r is a multiple of 4, we have the PTS with $M = NL/r$. However, there is one problem for the radix-r algorithm if r is determined by the choice of the first stage. To implement the radix-r algorithm it is required that NL has to be a power of r, which usually holds for $r = 2$ or 4 in the standardized systems (e.g. [18, 19]). The requirement comes from that the total number of stages in this algorithm, which is $m = \log_r NL$, must be an integer. To implement our proposed PTS schemes, it is likely that the values of r become very large and thus difficult to satisfy this requirement. To solve this problem, we observe that the output of stage 1 is fed into multiple (NL/r)-point IFFTs which may be implemented by radix-2 or radix-4 algorithm. To this end, we can first compute the first stage with radix-r and then the remaining using radix-2 or radix-4 algorithm as illustrated in Fig. 4.1. Hence, the

number of stage in our scheme is $m = 1 + \log_2 NL/r$ or $1 + \log_4 NL/r$. Notice that we choose radix-2 or radix-4 to implement the IFFT because they have less computational complexity in terms of multiplication compared with other radix-r algorithms.

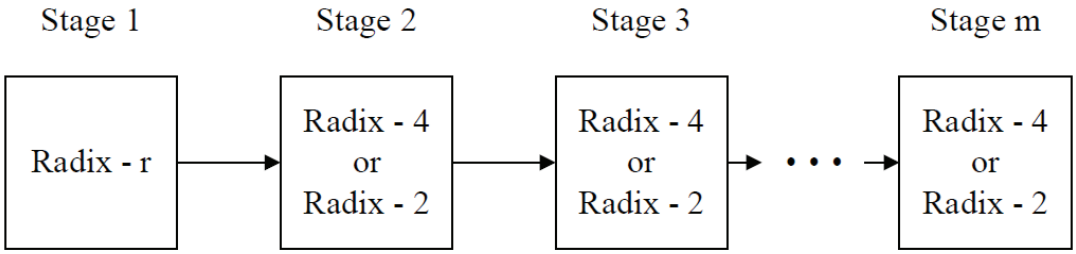

Figure 4.1: Architecture of the proposed scheme.

Unlike the conventional SLM and PTS schemes in which different phase sequences are applied respectively to an input data block and output sequences of IDFTs of disjoint subblocks, the proposed scheme calculates the multiplication of these phase sequences and the so-called *intermediate sequences*, which are the tentative output of the original data input in some stages. To generate multiple candidate sequences, we first divide the m stages into β subsets of stages where each subset contains one or several consecutive stages. Phase rotation is performed at the output of stages $v_D = [v_1, \cdots, v_\beta]$ with some designated phase sequences, where v_j denotes the output stage of the jth subset and v_1 is always set to be 1 in our algorithm. The numbers of intermediate signals, generated at stages v_D, are defined by $P_D = [P_1, P_2, \cdots, P_\beta]$ and increase successively. Figure 4.2 depicts the architecture of our proposed scheme, where P_j^i denotes the ith phase sequence applied to the intermediate sequence of output of stage v_j, for $i = 1, 2, \cdots, P_j$ and $j = 1, 2, \cdots, \beta$.

Accordingly, by the multiplication of stage 1 output and P_1 phase sequences, P_1 intermediate sequences at the output of stage 1 are obtained. Then, the output sequences are treated as the input of stage $v_1 + 1$ (i.e. 2) and are processed separately from stage 2 to v_2. Each of the P_1 intermediate sequences at the output of stage v_2 is then phase-

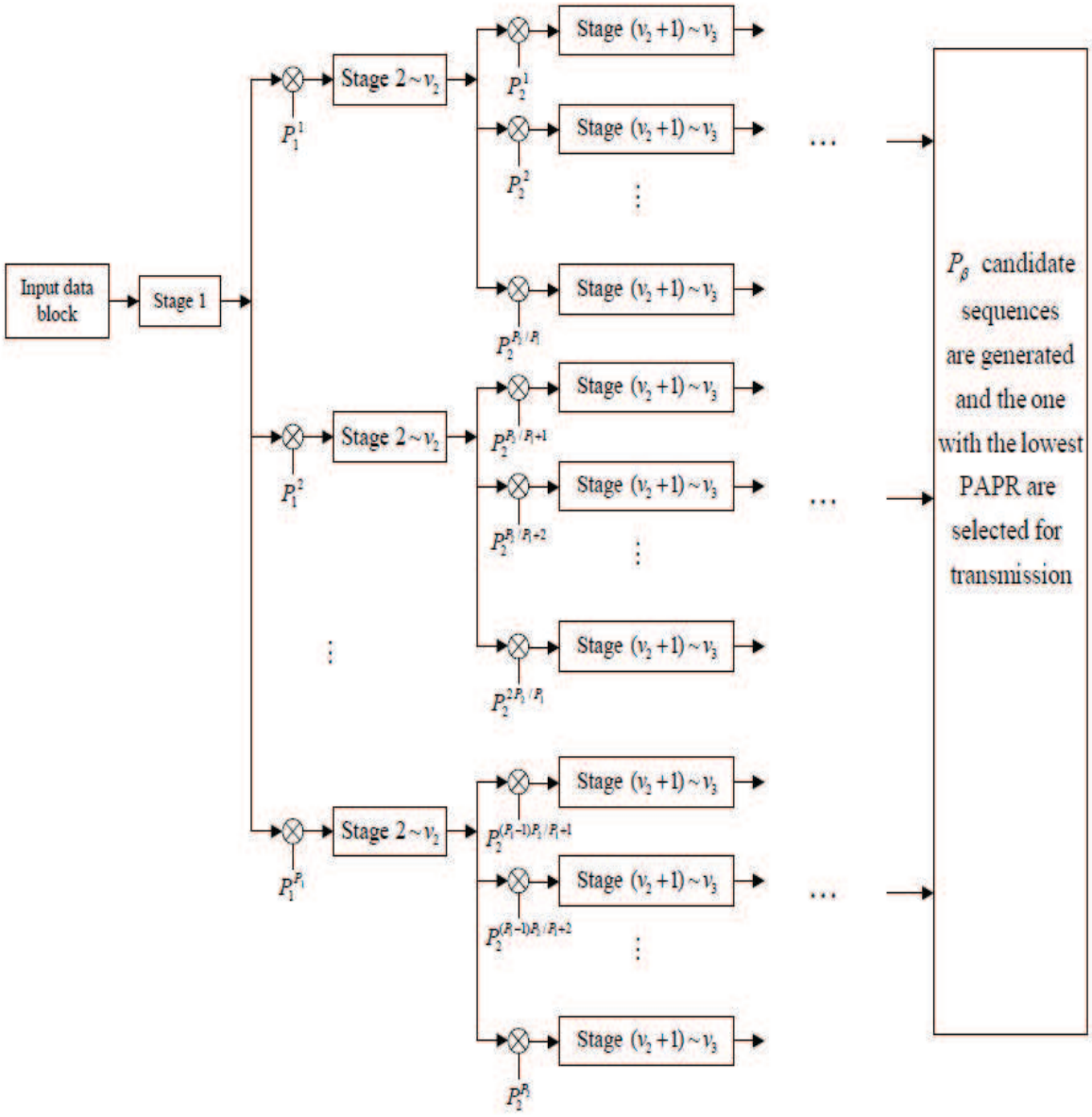

Figure 4.2: Detailed architecture of the proposed scheme.

rotated by P_2/P_1 phase sequences. Therefore, a total of P_2 new intermediate sequences are obtained after performing the operations of stage v_2. The same procedure of generating corresponding intermediate sequences is applied to subsequent stages repeatedly. Consequently, P_β candidate sequences are generated at the output of the last stage to lower PAPR. Compared with the conventional SLM or PTS schemes, the computation load of the new scheme is much relieved since phase sequences are multiplied to intermediate sequences. Here, we show a simple example of the proposed new SLM scheme for an OFDM system.

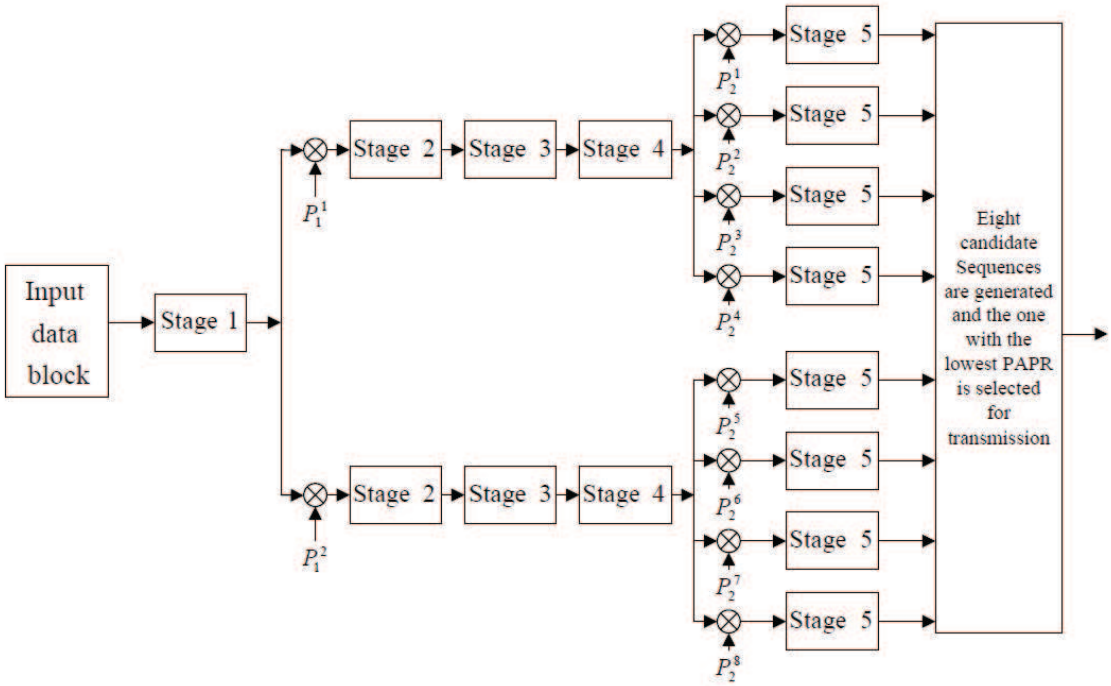

Figure 4.3: Block diagram of the proposed new SLM scheme with $v_D = [1, 4]$ and $P_D = [2, 8]$.

Example: Assume there are five stages of an IFFT operation for a given OFDM symbol, and $v_D = [1, 4]$ and $P_D = [2, 8]$ are configured to generate candidate sequences. Figure 4.3 presents the block diagram of this case. As we can see, two phase-rotated intermediate sequences are generated at the output of stage $v_1 = 1$ and individually computed through stage 2 to stage $v_2 = 4$. Subsequently, $P_2/P_1 = 4$ phase sequences

are applied to each of two intermediate sequences at the output of stage $v_2 = 4$ producing 8 intermediate sequences. Finally, the operation of stage 5 is performed at all 8 intermediate sequences separately to generate a total of $P_2 = 8$ candidate sequences.

4.2.2 Phase sequences of new SLM and PTS Schemes

For convenience, we consider radix-2 here. The extension to radix-4 or the hybrid of radix-2 and radix-4 is straightforward. Recall that the operations at a certain stage of DIT radix-r IFFT are performed by a number of linear combinations. Hence, each subcarrier data is a specific element of linear combinations appears $r \cdot 2^{(v-1)}$ times at stage v in the multistage structure. In order to avoid the degradation of bit error rate (BER) performance, this sample must be multiplied by the same phase factor whenever it appears at stage v to maintain its power. In other words, the phase sequences with length $NL/(r \cdot 2^{(v-1)})$ is applied to the output sequence of stage v, and all $r \cdot 2^{(v-1)}(NL/(r \cdot 2^{(v-1)}))$-point IDFT output sequences are multiplied by the same phase sequence to generate a corresponding intermediate sequence.

As for the G&G SLM scheme, the phase factors multiplied to the intermediate samples containing the same data are unnecessarily identical. Thus, the equivalent effect on that data is a linear combination of these phase factors which cannot guarantee the data power unchangeable anymore. To visualize such effect, the magnitude of an equivalent phase sequence of the proposed and G&G SLM schemes are depicted in Fig. 4.5 and 4.6 with $N = 256$ employed.

4.3 Performance Analysis and Comparison

4.3.1 Computational Complexity Analysis

In our proposed scheme, phase sequences are multiplied by the intermediate sequences at the output of stages $v_D = [1, v_2, \cdots, v_\beta]$ with the corresponding numbers of

sequences given by $P_D = [P_1, P_2, \cdots, P_\beta]$, respectively. Hence, the total number of IFFT stages required to generate P_β candidate sequences excluding the first stage is

$$\lambda = (v_2 - 1) \cdot P_1 + (v_3 - v_2) \cdot P_2 + \cdots + (m - v_\beta) \cdot P_\beta, \tag{4.2}$$

where m is the total number of stages to generate a specific candidate sequence:

$$m = 1 + \log_2 \frac{NL}{r}. \tag{4.3}$$

Since the computational complexity is fixed in each stage ($NL/2$ multiplications and NL additions), we have the complexity analysis of our scheme, stated in Table 4.1 – **??**.

The G&G SLM scheme, which make use of the multistage structure of radix-2 IFFT, applies phase sequences differently from ours. Their operation of phase rotation is considered at the output of stages $v_R = [v_1, v_2, \cdots, v_\beta]$ and done to $P_R = [P_1, P_2, \cdots, P_\beta]$ intermediate sequences, where P_R is defined as the number of intermediate sequences generated at stages v_R. Thus, the total number of stages required (including the first few stages) is given as

$$\lambda_R = v_1 + (v_2 - v_1) \cdot P_1 + \cdots + (m_R - v_\beta) \cdot P_\beta, \tag{4.4}$$

where $m_R = \log_2 NL$. For fair comparison, radix-2 is considered for the last $m-1$ stages of our proposed scheme, where it is done to all IFFT stages in the G&G SLM scheme. Note that though the value of m and m_R are different, the computational complexity of our proposal with $r = 4$ at the first stage and the that of the G&G SLM scheme is identical if same numbers of phase sequences are applied to the corresponding stages.

Table 4.1 – 4.2 present the computational complexity of our proposed schemes, the G&G SLM scheme, and the conventional SLM schemes. In addition, the computational complexity ratio of the proposed schemes over the conventional schemes are shown in Table 4.3 for $N = 256$. Obviously, the complexity is reduced.

Table 4.1: Computational complexity of various SLM schemes (I)

	Number of complex multiplications
Conventional SLM scheme	$U\left(\frac{NL}{2} \cdot \log_2 NL\right)$
Proposed SLM scheme	$NL + \frac{NL}{2} \cdot \lambda$
G&G SLM scheme	$\frac{NL}{2} \cdot \lambda_R$

Table 4.2: Computational complexity of various SLM schemes (II)

	Number of complex additions
Conventional SLM scheme	$U(NL \cdot \log_2 NL)$
Proposed SLM scheme	$NL(1 + \lambda)$
G&G SLM scheme	$NL \cdot \lambda_R$

4.3.2 Simulation Results

The comparison of PAPR reduction performance of various schemes is presented in this section. The evaluation considers the CCDF of the PAPR of 16 QAM-modulated OFDM symbols with $U = 8$ and $N = 256$.

The PAPR reduction performance of various SLM schemes is depicted in Fig. 4.4, where v_D and v_R denote the stages phase sequences are multiplied for our scheme and the G&G scheme, respectively. As can be seen, the earlier the phase sequences are applied to, the better the PAPR reduction performance. This observation coincides with the intuition that the multiplication of phase sequences of the earlier stages introduces more diversity to the candidates. However, the cost of improving PAPR reduction capability is the higher computational complexity; as shown in Table 4.3. This gives us a direct trade-off between the PAPR performance and computational complexity which is beneficial for system design. Notice that when $v_D = [1, 4]$ is applied in our proposed scheme, it can achieve almost the same performance as the conventional SLM scheme with a complexity ratio of 60% only. This shows the potential improvement of complexity reduction with negligible performance degradation by joint design. From Table 4.1 and 4.2, the computational complexity of $v_D = [1, 6]$ in our proposed scheme and $v_R = [2, 7]$

Table 4.3: Computational complexity ratio of the proposed SLM schemes with $N = 256$.

v_D	P_D	R_{mul} (%)	R_{add} (%)
$[1, 4]$	$[2, 8]$	60.00	58.75
$[1, 6]$	$[2, 8]$	45.00	43.75
$[1, 8]$	$[2, 8]$	30.00	28.75

in the G&G SLM scheme are identical while shown in Fig. 4.4 the PAPR reduction performance of the latter is poorer than the former with 0.12 dB for $U = 8$ at the CCDF of 10^{-4}, which shows the advantage of our scheme over G&G SLM scheme. The case with $v_D = [1, 8]$ has the worst PAPR reduction performance among all three cases since the second part of the phase sequences are multiplied to a later stage to obtain the lowest complexity.

As mentioned in previous subsection, to guarantee the BER performance, our proposed schemes have to follow some rules to ensure the factors of equivalent phase sequences all locate on the unit circle while the G&G SLM scheme does not take into account. Figure 4.5 and 4.6 show the magnitudes of equivalent phase sequences of our scheme and the G&G SLM scheme, respectively. These results conform to what we discussed before. To investigate the effect of destroying the unimodularity, the BER performance of our SLM scheme and the G&G SLM scheme is also given in Fig. 4.7 where a 256-subcarrier QPSK-modulated OFDM system is considered. As our expectation, the BER performance of the G&G SLM scheme is much poorer than our proposal.

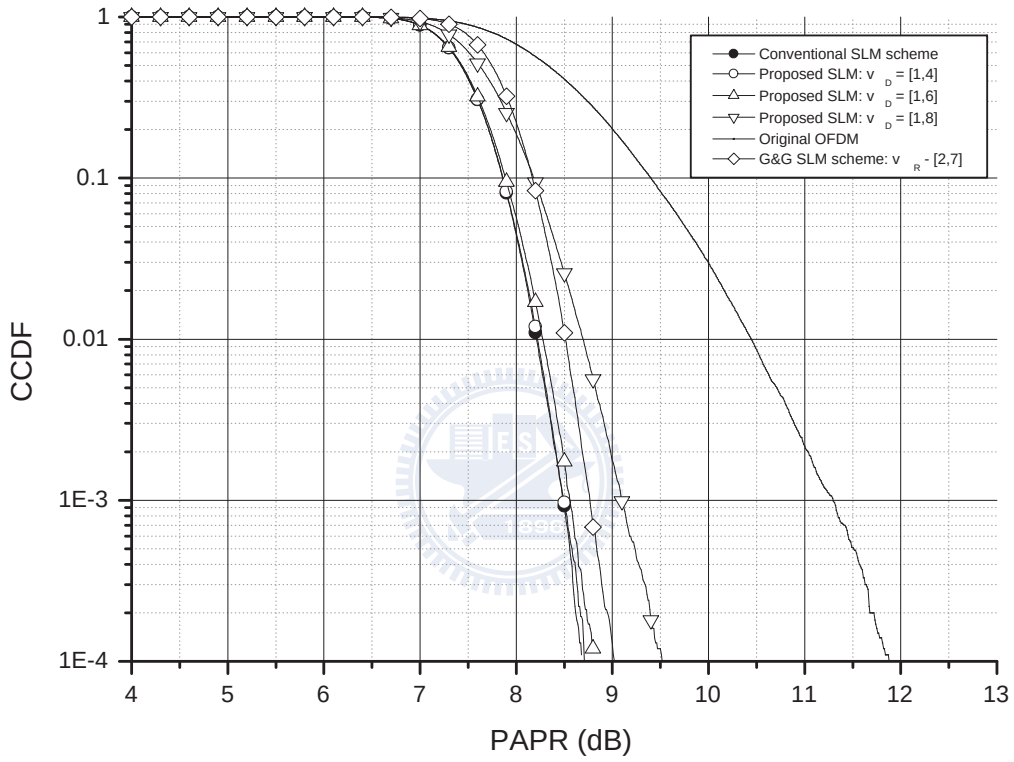

Figure 4.4: Comparison of the PAPR reduction performance of the proposed SLM Scheme, G&G SLM scheme and conventional SLM scheme.

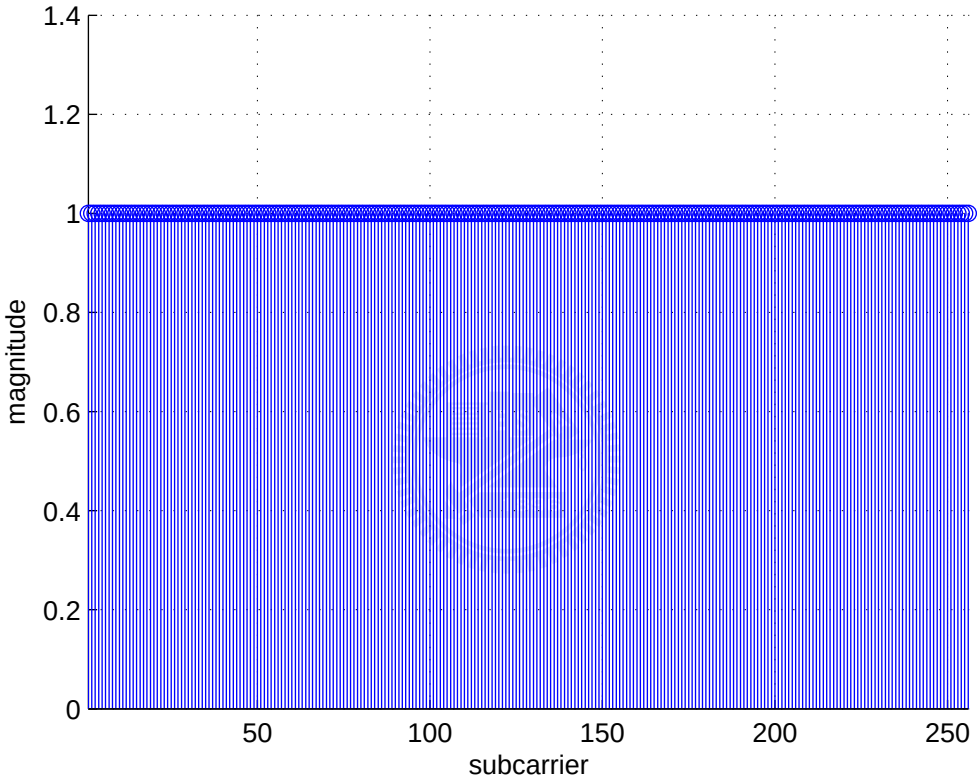

Figure 4.5: Magnitude of an equivalent phase sequence of our scheme.

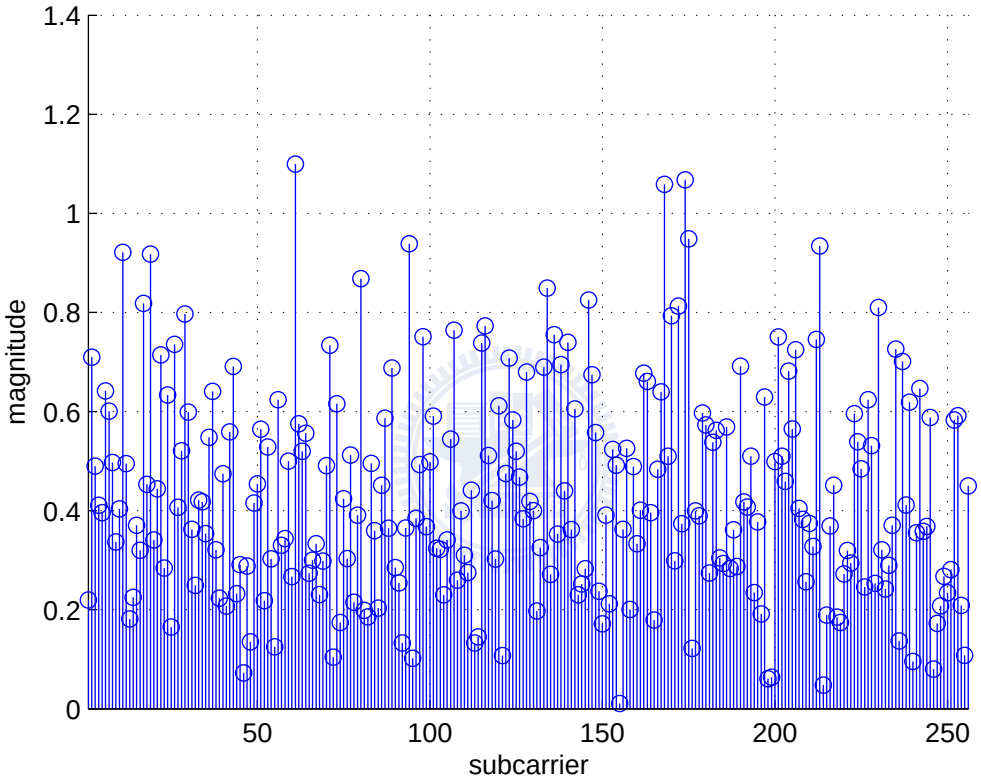

Figure 4.6: Magnitude of an equivalent phase sequence of the G&G SLM scheme.

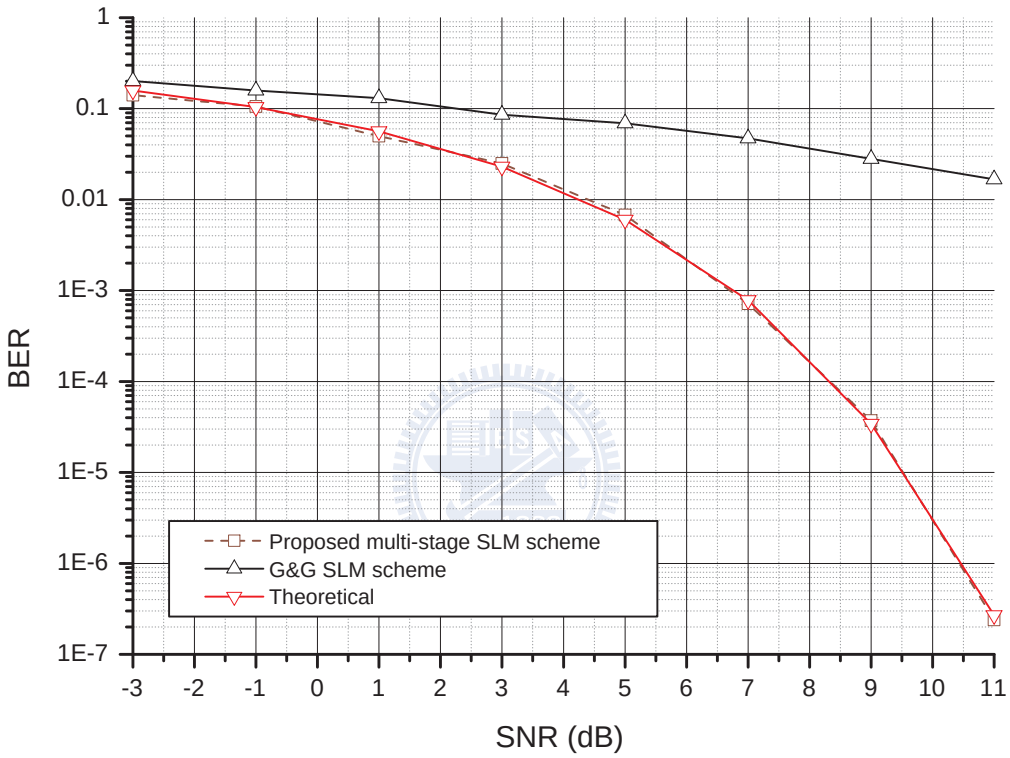

Figure 4.7: Comparison of the BER performance of the proposed SLM Scheme and the G&G SLM scheme.

Chapter 5

Conclusion

Several novel low complexity SLM-based and PTS-based schemes for PAPR reduction are proposed. These schemes make use of some special properties of the IFFT structures which are known as DIT IFFT or DIF IFFT. We also suggest a stop criterion to further reduce the computational complexity for the DIT-IFFT implementation.

The new schemes achieve the same PAPR reduction performance as the conventional schemes with much reduced computational complexity. For instance, when the number of subcarriers (N) is 256 and the number of mapping sequences (U) is 8, the multiplication complexity ratios (normalized with respect to that required by the conventional SLM/PTS schemes) are 82.5% and 60% for the SLM and PTS (which uses four sub-blocks) schemes, respectively. If the stop criterion is applied, the reduction ratio can be further improved. Besides variants of the conventional SLM and PTS schemes, we can apply the proposed stop criterion to reduce the complexity of the LWW schemes [12] as well.

We extend our study to the multistage DIT IFFT structure. A similar approach, which we referred to as the G&G SLM scheme [16], was presented before. A shortcoming of this scheme is that the equivalent mapping sequence does not have constant modulus entries and, as a result, the receiver's de-mapping process brings about noise enhancement and BER performance degradation. Our new design overcomes this disadvantage

by generating multiple constant modulus candidate frequency domain sequences.

The concept of taking advantage of the special IFFT structures in designing new PAPR reduction schemes can be extended to modify other existing PAPR reduction schemes and develop new low-complexity schemes. One such example is the bit-flipping based PAPR reduction schemes. Moreover, as there are several recent proposals for simplifying the implementation of IDFTs, it is worthwhile to consider these alternative structures, e.g., split-radix FFT algorithm, and investigate the feasibility of further computational complexity reduction when used in conjunction with some PAPR reduction schemes.

Bibliography

[1] S. Han and J. Lee, "An overview of peak-to-average power ratio reduction techniques for multicarrier transmission", *IEEE Trans. Wireless Commun,* vol. 12, no. 2 , Apr. 2005, pp. 56-65.

[2] A. E. Jones, T. A. Wilkinson, and S. K. Barton, "Block Coding Scheme for Reduction of Peak to Mean Envelope Power Ratio of Multicarrier Transmission Scheme," *Electron. Lett.,* vol. 30, no. 22, Dec. 1994, pp. 2098-2099.

[3] R. O'Neill and L. B. Lopes, "Envelope Variations and Spectral Splatter in Clipped Multicarrier Signals," in *Proc. IEEE PIMRC '95,* Toronto, Canada, Sep. 1995, pp. 71-75.

[4] B. S. Krongold and D. L. Jones, "PAR Reduction in OFDM via Active Constellation Extension," *IEEE Trans. Broadcast.,* vol. 49, no. 3, Sep. 2003, pp. 258-268.

[5] J. Tellado, "Peak to Average Power Reduction for Multicarrier Modulation," Ph.D. dissertation, Stanford Univ., 2000.

[6] R. W. Bauml, R. F. H. Fischer, and J. B. Huber, "Reducing the Peak-to-Average Power Ratio of Multicarrier Modulation by Selective Mapping," *Electron. Lett.*, vol. 32, no. 22, Oct. 1996, pp. 2056-2057.

[7] S. H. Müller and J. B. Huber, "OFDM with Reduced Peak-to-Average Power Ratio by Optimum Combination of Partial Transmit Sequences," *Electron. Lett.*, vol. 33, no. 5, Feb. 1997, pp. 368-369.

[8] C. Tellambura, "Computation of the Continuous-Time PAR of an OFDM Signal with BPSK Subcarriers," *IEEE Commun. Lett.*, vol. 5, no. 5, May 2001, pp. 185-187.

[9] K. Daniel Wong, Man-On Pun and H. Vincent Poor, "The Continuous-Time Peak-to-Average Power Ratio of OFDM Signals Using Complex Modulation Schemes," *IEEE Trans. Commun.*, vol. 56, no. 9, Sep. 2008.

[10] R. van Nee and R. Prasad, *OFDM Wireless Multimedia Communications*, Artech House, 2000.

[11] C. L. Wang and Y. Ouyang, "Low-Complexity selected mapping schemes for peak-to-avarage power ratio reduction in OFDM systems," *IEEE Trans. Signal Process.*, vol. 53, no. 12, pp. 4652-4660, Dec. 2005.

[12] C. P. Li, S. H. Wang, and C. L. Wang, "Novel Low-Complexity SLM Schemes for PAPR Reduction in OFDM Systems," *IEEE Trans. Signal Process.*, vol. 58, no. 5, pp. 2916-2921, May 2010.

[13] C. P. Li and W. C. Huang, "A constructive repersentation for the Fourier dual of the Zadoff-Chu sequences," *IEEE Trans. Inf. Theory*, vol. 53, no.11, pp. 4221-4224, Nov. 2007.

[14] H. V. Sorensen and C. S. Burrus, "A new efficient algorithm for computing a few DFT points," presented at the *IEEE 1988 Int. Symp. Circuits Syst.*, pp. 1915-1918, Jun. 7-9, 1988.

[15] G. Goertzel, "An algorithm for the evaluation for finite trigonometric series," *Amer. Math. Monthly*, vol. 65, pp. 34-35, Jan. 1958.

[16] A. Ghassemi and T. A. Gulliver, "A Low Complexity SLM-Based Radix FFT Method for PAPR Reduction in OFDM Systems," presented at the *IEEE Pacific*

Rim Conference on Communications, Computers and Signal Processing, pp. 304-307, Aug. 22-24, 2007.

[17] A. Ghassemi and T. A. Gulliver, "A Low-Complexity PTS-Based Radix FFT Method for PAPR Reduction in OFDM Systems," *IEEE Trans. Signal Process.* vol. 56, no.3, pp. 1161-1166, Mar. 2008.

[18] F. Wang, A. Ghosh, C. Sankaran and P. Fleming, "WiMAX Overview and System Performance," presented at the *IEEE Vehicular Technology Conference 2006 Fall*, Montreal, Canada, Sep. 2006.

[19] A. Ghosh, R. Ratasuk, B. Mondal, N. Mangalvedhe and T. Thomas, "LTE-advanced: next-generation wireless broadband technology," *IEEE Trans. Wireless Commun.*, pp. 10-22, Jun. 2010.